



Application of a novel biochar adsorbent and membrane to the selective separation of phosphate from phosphate-rich wastewaters



Rubaba Mohammadi^{a,*}, Masoumeh Hezarjaribi^{a,b}, Deepika Lakshmi Ramasamy^a, Mika Sillanpää^{c,d,e,f}, Arto Pihlajamäki^g

^a Department of Separation Science, Lappeenranta-Lahti University of Technology, Sammonkatu 12, FI-50130 Mikkeli, Finland

^b Faculty of Chemical Engineering, Babol Noshirvani University of Technology 47148-71167 Shariati Ave., Babol, Mazandaran, Iran

^c Institute of Research and Development, Duy Tan University, Da Nang 550000, Viet Nam

^d Faculty of Environment and Chemical Engineering, Duy Tan University, Da Nang 550000, Viet Nam

^e School of Civil Engineering and Surveying, Faculty of Health, Engineering and Sciences, University of Southern Queensland, West Street, Toowoomba 4350, QLD, Australia

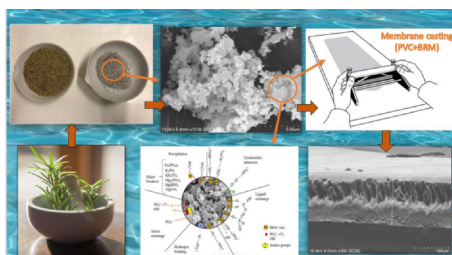
^f Department of Chemical Engineering, School of Mining, Metallurgy and Chemical Engineering, University of Johannesburg, P. O. Box 17011, Doornfontein 2028, South Africa

^g School of Engineering Science, Lappeenranta-Lahti University of Technology, Lappeenranta 53851, Finland

HIGHLIGHTS

- Biochar from *Rosmarinus officinalis* leaves (BRM) was employed in this study.
- Adsorptive mixed matrix membrane (PVC-BRM) was fabricated by incorporating BRM.
- BRM and PVC-BRM membranes exhibited high phosphate removal efficiencies.
- The PVC-BRM membrane showed higher reusability than BRM adsorbent.
- BRM exhibits excellent separation of phosphate from different wastewaters.

GRAPHICAL ABSTRACT



ARTICLE INFO

Keywords:

Biochar
Phosphate
Membrane separation
Recovery

ABSTRACT

A novel biochar from *Rosmarinus officinalis* leaves (BRM) was employed for phosphate removal and recovery and compared with ZnO as a reference. Further, an adsorptive mixed matrix membrane suitable for practical adsorption applications in industry was fabricated by incorporating BRM particles in a polymeric matrix (PVC-BRM). The adsorption capacity of the BRM was tested by isotherm and kinetic experiments, and the adsorption properties of the membranes were evaluated by filtration experiments in a cross-flow system. Both BRM and PVC-BRM were characterized by analyzing their morphology and composition. The maximum adsorption capacity of BRM was 78.24 mg/g, and the adsorption of phosphate was endothermic and obeyed the Langmuir and Freundlich isotherms, indicating that multiple mechanisms are involved in the adsorption. BRM and PVC-BRM exhibited high removal efficiencies toward phosphate in a wide range of single and multi-component solutions. In a multi-component system, phosphate displayed preferential adsorption for BRM; in PVC-BRM, however, phosphate selectivity decreased. The adsorption of phosphate was pH-dependent and was enhanced in acidic conditions. The adsorption capacity increased with higher initial phosphate concentration for BRM and PVC-BRM, although removal efficiency decreased. Desorption efficiency was low in both BRM and PVC-BRM;

* Corresponding author.

E-mail address: Rubaba.Mohammadi@lut.fi (R. Mohammadi).

<https://doi.org/10.1016/j.cej.2020.126494>

Received 17 June 2020; Received in revised form 26 July 2020; Accepted 28 July 2020

Available online 02 August 2020

1385-8947/ © 2020 The Author(s). Published by Elsevier B.V. This is an open access article under the CC BY license

(<http://creativecommons.org/licenses/by/4.0/>).

however, 75% regeneration was achieved by NaOH in BRM. The membrane showed higher reusability than BRM. Adsorption mechanism studies revealed that the removal of phosphate was associated with ion exchange, electrostatic interaction, hydrogen bonding, ligand exchange, and precipitation with metal oxides and hydroxides. Besides, BRM exhibits excellent selective separation of phosphate from different wastewaters and agriculture runoff as secondary resources.

1. Introduction

Phosphorous (P) is a limiting nutrient in freshwater systems that even at low concentrations of 0.01 to 0.1 mg/L P can cause excess algae growth and eutrophication, which damage water resources and harm aquatic flora and fauna, and human well-being [1,2,3,4,5,6]. Wastewater treatment plants (WWTPs), industrial activities, and agricultural runoff are common sources of P discharge to water bodies. On the other hand, while phosphorus is detrimental to aquatic environments, it is a critical nutrient for agricultural products. Furthermore, it is a limited resource, and phosphate fertilizers are currently produced naturally extracted from non-renewable phosphate rocks located in only a few places in the world. These resources could be depleted in the next 50–100 years, consequently have an adverse effect on long-term food security and agricultural production [7,8]. Phosphate extraction and removal from secondary sources can improve resource security, reduce the exploitation of natural phosphorus, mitigate eutrophication in water bodies, and address other related environmental issues [9,10].

Various techniques have been applied for phosphate removal from water and wastewater, for example, biological treatment [11,12], chemical precipitation [13,14,15], ion exchange and adsorption [2,16,17]. Although the different methods are able to remove phosphate, each technique has some drawbacks. Biological treatment is a highly efficient method, but it is costly and sensitive to many external factors [2,18]. Chemical precipitation is currently the most common process since it is cost-effective; nevertheless, it produces vast quantities of sludge, which causes secondary pollution, and pH control in this process is challenging [2,19,20,21]. The use of traditional ion exchangers suffers from limited efficiency, due to the low concentration of phosphate ions present in municipal wastewater effluents compared to other anions [22]. Adsorption, however, can be considered a preferred technique on account of its simple operation, design flexibility, and lack of sludge production [16,18,23]. To date, many types of adsorbents from various component have been evaluated for the removal of phosphate from aqueous solutions, such as layered double hydroxide [24], nanoparticles [25,26,27], lanthanum [28,29,30], ferric oxide [31], zirconium oxide [32,33] and zero-valent iron [34]. However, many of these adsorbents have either insufficient phosphate adsorption capacity, complicated and expensive synthesis and manufacturing processes, or harmful environmental effects due to the production of toxic, acidic or alkaline waste in the adsorbent manufacturing process [35,36].

A number of studies have shown that biochars formed from the pyrolysis of organic materials adsorb various ions, including phosphates ($\text{PO}_4^{3-}\text{-P}$) [37,38,39,40]. However, unmodified biochars have been reported as having insufficient P adsorption capacity and presented that additional chemicals are needed for modification [41,42,43].

A novel and promising highly selective phosphate adsorbent is biochar from *Rosmarinus officinalis* leaves (BRM), whose use for the recovery of P has not previously been reported in the literature. *Rosmarinus officinalis* (RM) is an abundant material that is widely found and easily grown. Additionally, the preparation method for BRM is simple and does not require the use of additional chemicals that make it applicable in many environments, from small wastewater treatment plants in remote areas to large industrial operations. Furthermore, biochar is a bio-based, cheap, and non-toxic adsorbent that can be used as slow-release fertilizer in the soil.

Many adsorbents, however, are of small size, which means that

additional treatment processes are required to separate fine adsorbent particles from wastewater to prevent clogging in pipes or pumps of treatment plants [44]. One promising technology is the mixed matrix membrane (MMM), which comprises inorganic fillers dispersed in a polymer matrix. The combined effects of the polymeric matrix and solid particles [45] facilitate the utilization of dispersed adsorbents and enhance the mechanical properties of the polymers [46]. Moreover, MMM can be used as a single treatment procedure without needing to separate adsorbents. Recently there has been an increased interest and research works in functionalized and preparing mix matrix membranes [47,48,49,50,51,52,53]; however, there is limited research work on selective phosphate membrane.

Therefore, the aim of this study was initially to apply BRM as a phosphate selective adsorbent or selector to separate and recover phosphate from the solution. In the next step, a porous embedded polyvinyl chloride (PVC) mixed matrix membrane with BRM was developed and tested as a practical approach for BRM application in the water treatment industry. The study additionally investigates P uptake by BRM from different wastewaters and agricultural runoff to address the challenges of removing P at the low concentrations (0.1–20 mg/L PO_4^{3-}) found in many wastewaters. Zinc oxide (ZnO) nanoparticles have been reported as an effective adsorbent for phosphate removal in the research literature [54,55,56], and ZnO is thus used as a comparative adsorbent for the batch adsorption and filtration experiments in this work.

Analytical techniques are used to characterize the adsorbents and membranes before and after phosphate treatment, and the possible removal mechanism is discussed. The performance of the adsorbents and MMMs in phosphate removal is evaluated using isotherm and kinetic models, and the effect of pH, competing anions, initial phosphate concentration and adsorbent loading on the membrane are assessed. In further study, desorption and regeneration of P as adsorbent and membrane and the risk of heavy metal leaching from the biochar were evaluated to consider their potential reuse as fertilizer or for other purposes.

2. Experimental

2.1. Materials

RM was purchased from a local shop in Finland and pyrolyzed at 500 °C for 2 h in a muffle furnace under limited oxygen conditions. The char produced was allowed to cool to room temperature and ground to a fine powder by tube mill (IKA Tube Mill Control) and sieved with a 150 μm mesh. N-methyl-2-pyrrolidone (NMP) was used as the solvent, and polyvinyl chloride (PVC) (average $M_w \sim 80,000$) was used as the polymer. ZnO < 100 nm (M_w 81.39) and all chemicals used were of analytical grade, purchased from Sigma Aldrich, and were used without further purification.

2.2. Characterization and analysis

The crystalline structure of the prepared BRM and ZnO before and after phosphate adsorption were identified by X-ray diffraction (X-Ray Diffractometer, Empyrean Series 2 (PANalytical, 2014) with Cu K α radiation. Additionally, Fourier transform infrared spectroscopy (FTIR, Bruker Vertex 70 spectrometer) was used to analyze the functional groups of sorbents and their changes after adsorption. The chemical

composition and chemical bonding of the samples were analyzed using a Thermo Fisher Scientific ESCALAB 250Xi XPS System. The surface morphology and elemental composition of the adsorbents and membranes were analyzed using scanning electron microscopy and energy-dispersive X-ray spectroscopy (SEM-EDS) (Hitachi S-4800). The surface area and porosity of sorbents were determined by Brunauer–Emmett–Teller (BET) method using the nitrogen adsorption–desorption isotherm at 600 °C degassing temperature (Micromeritics Tristar II Plus analyzer). Phosphate and other anion concentrations in the aqueous samples and wastewater were determined by ion chromatography (IC SI-50 4E: column size: 4 mm ID 250 mm, flow rate: 0.7 mL min⁻¹, detector: suppressed CD). Cations concentrations in the aqueous samples were detected by ion chromatography (IC YS-50: column size: 4.6 mm ID 125 mm, flow rate: 1 mL/min). Heavy metal traces were determined by ICP-OES analysis (Agilent ICP-OES 5110). The zeta potentials of the BRM were measured in a Zetasizer (Malvern ZEN3500 Zetasizer Nano ZS) with MilliQ water as the carrier fluid. Water content, porosity, and pore size of the membranes were calculated as described in [Text S1](#) in [supplementary data](#).

2.3. Membrane preparation

For the membrane preparation, both BRM and ZnO hybrid membranes were prepared. Firstly, a casting solution of 20 wt% PVC was prepared by mixing polymer in NMP and stirring for 48 h. Subsequently, different amounts of BRM and ZnO were dispersed into the polymeric solutions, and stirring continued to obtain a homogeneous casting solution. 1 h sonication and 30 min degassing were used to obtain well-dispersed solution and to remove air bubbles. Using a film applicator, the prepared solutions were cast onto clean glass plates with a thickness of 150 μm. The glass plates were immersed in distilled water for 24 h to remove the solvent and were then dried at room temperature.

2.4. Adsorption experiments

For the different phosphate adsorption experiments, a stock solution of 10 mM was prepared and then diluted to produce solutions with various phosphate concentrations. For the isothermal adsorption experiments, 125 mg of adsorbents were added into 100 mL PO₄³⁻ solutions in a conical flask, followed by stirring. The solutions were mixed for 1 hr at a rotation speed of 200 rpm and temperature of T = 25, 35, 45 °C using an orbital shaker (KS IKA 4000). The experiments were carried out in triplicate, and BRM from each sample were combined for the desorption experiments. Kinetics studies were carried out similarly with different initial concentrations of 40, 80, 160 mg/L PO₄³⁻ at

different contact times (0–75 min). The effect of pH on phosphate adsorption was analyzed with initial pHs of 3, 5, 7 and 9 using a 1 M HCl and 1 M NaOH solution. To study the effect of competitive anions on adsorption, 125 mg of adsorbents were introduced into 100 mL of mixed solution with an equal concentration of 1 mM of SO₄²⁻, NO₃⁻, Cl⁻, and PO₄³⁻ anions.

The residual PO₄³⁻ and other ion concentrations in the samples were analyzed using ion chromatography (Shimadzu IC). The value of PO₄³⁻ adsorbed (q_e, mg/g) per unit weight of adsorbent and the removal efficiency (E) of the adsorbents were calculated using Eqs. (1) and (2), respectively:

$$q_e = \left[\frac{C_0 - C_e}{m} \right] V \quad (1)$$

and:

$$E(\%) = \left[\frac{C_0 - C_e}{C_0} \right] \times 100 \quad (2)$$

where C₀ and C_e are the primary (mg/L) and final concentrations (mg/L) of PO₄³⁻ in the solution, respectively, V is the volume (L) of the PO₄³⁻ solution, and m is the mass (g) of dry adsorbents [57,58,59]. The partition coefficient (PC) was calculated as follows:

$$PC = \frac{q_e}{C_e} \quad (3)$$

where C_e is the final concentrations of PO₄³⁻ in the solution base on μM [58].

2.5. Filtration experiments

A cross-flow ultrafiltration setup containing a rectangular membrane module with an effective dimension of 40x80 mm was used to perform phosphate removal and to measure the separation capacity of the membranes. An overview of the UF system is shown in [Fig. S1](#) in [supplementary data](#). Water flux and removal assessment were performed at a fixed pressure of 1 bar and permeate flow rate of 1–2 mL/min. Prior to the experiments, membranes were soaked in diluted ethanol and DI water for 15 min, respectively, then compacted in the system by filtering DI water for 1 h. 1 L of feed solution containing PO₄³⁻ or multi-component solution was used for the filtration tests. The removal efficiency (E) of the membrane were calculated by means of Eqs. (5), where C_e is the final concentrations of PO₄³⁻ in the permeate solution.

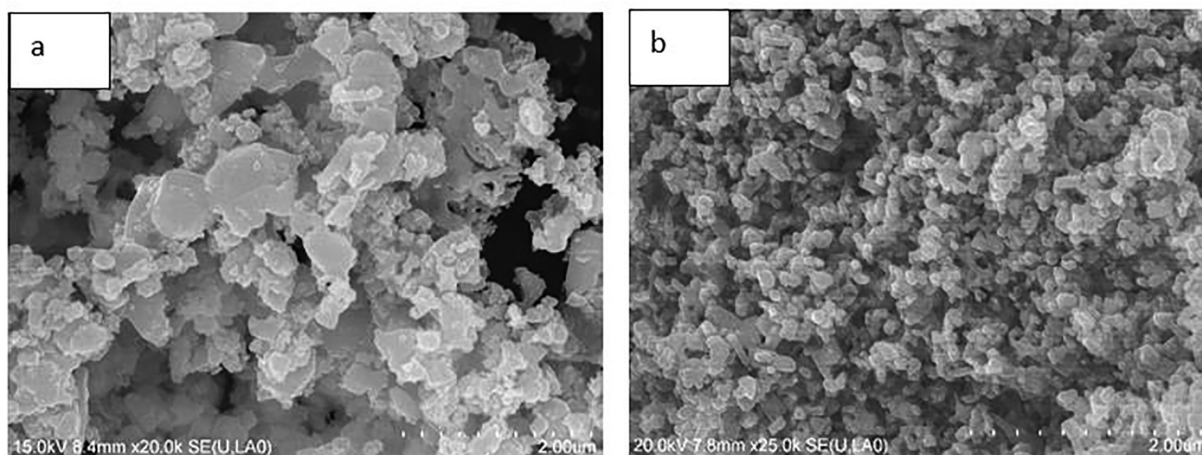


Fig. 1. Surface images of adsorbents, (a) BRM (b) ZnO.

2.6. Adsorbent and membrane regeneration

The phosphate loaded BRM was collected and then dried in an oven. Then the dried BRM regenerated by NaCl and NaOH solutions agitating for 20 min. The regenerated biochar was filtrated through quantitative filter paper and washed with DI water several times until the pH neutral and then dried for reusing in the cycle of adsorption–desorption. The recovery solutions were then collected and filtered for the detection of phosphate released from the regenerated BRM. Furthermore, the used membranes were regenerated by filtration of 1 M NaCl for 20 min and then washed thoroughly by 20 min DI water filtration.

3. Results and discussion

3.1. Characterization and morphology of adsorbents and membrane

SEM: Fig. 1 displays SEM images of ball-milled BRM and ZnO. The corresponding EDS analysis is shown in Figs. 3 and 4, respectively. Based on the SEM images shown in Fig. 1, BRM appears to have a heterogeneous surface morphology with varying particle sizes that seem to be bigger than ZnO particles. The ZnO particles display sheet-like morphologies, and the particles are of different sizes.

Fig. 2 shows SEM images of the top surface and cross-section of prepared membranes with different loading of adsorbents in the casting solution. As can be observed from the cross-section, all membranes have the “finger-like” type structure supported by a thick sub-layer that is characteristic of membranes prepared by Non-solvent Induced Phase Inversion (NIPS) method. The morphology of the membrane is influenced by kinetics and thermodynamics of the polymer/solvent/non-solvent system [60,61]. These finger-like pores gradually decreased with increasing adsorbents loading and purging, especially in 15 wt% ZnO (Fig. 3. f2), after which an almost entirely sponge-like structure can be observed. Higher adsorbents dispersal increases the viscosity of the casting solution, which might be a reason for the sublayer

morphology changes, and greater dispersal may also reduce the replacement rate between NMP and water during the phase inversion process [44,61,62]. The membrane surfaces had porous microstructures, and adsorbent particles were observed along the membranes, indicating that the particles were evenly dispersed on the membranes even at high adsorbents loading. In Fig. 2, it can be seen that as the adsorbent loading on the membranes increases, more adsorbents are found on the surface. Furthermore, the size of the BRM particles is bigger than that of the ZnO nanoparticles, which is in agreement with BET results and Fig. 1.

EDS: The EDS spectrum indicates that the main components in BRM are C, O, N, Ca^{2+} , K^+ , and Mg^{2+} , respectively (Fig. 3), which is in approximate agreement with biochar components in other studies [63,64,65]. The content of C, H, and N in BRM in the elemental analysis were 24.32%, 0.87%, and 1.31%, respectively, which differs slightly from the EDS ratio. The EDS of the ZnO nanoparticle (Fig. 4) has element peaks of the Zn and O signals at an approximate atomic ratio of 58.39:20.3, which is consistent with the stoichiometry of ZnO. The atomic percentage of approximately 37.43% carbon in the EDS analysis and 24.32% carbon in the elemental analysis confirmed that carbon structures dominated the composition of the biochar. The second and the third most dominant elements in BRM are O and N with an atomic percentage of 29.56% and 15.95% in the EDS analysis, which might be due to the presence of amine groups; the elemental analysis, however, showed 1.32% nitrogen in the BRM composition. The higher amount of N and possibly amine group in this study was not observed in other biochar studies [38,40,43,66] that might be the reason for the higher phosphate adsorption rate with our unmodified BRM. Ca^{2+} is the other dominant metal element in the BRM; Ca^{2+} has also been observed in other biochar studies [64,65]. Metal elements such as Ca^{2+} , Mg^{2+} , and K^+ found in biochars originate from the ash [67], that these metals are positively associated with the phosphate uptake capacity of biochars [65,66]. The higher amount of metals observed in our BRM would be the other reason for enhancing phosphate adsorption

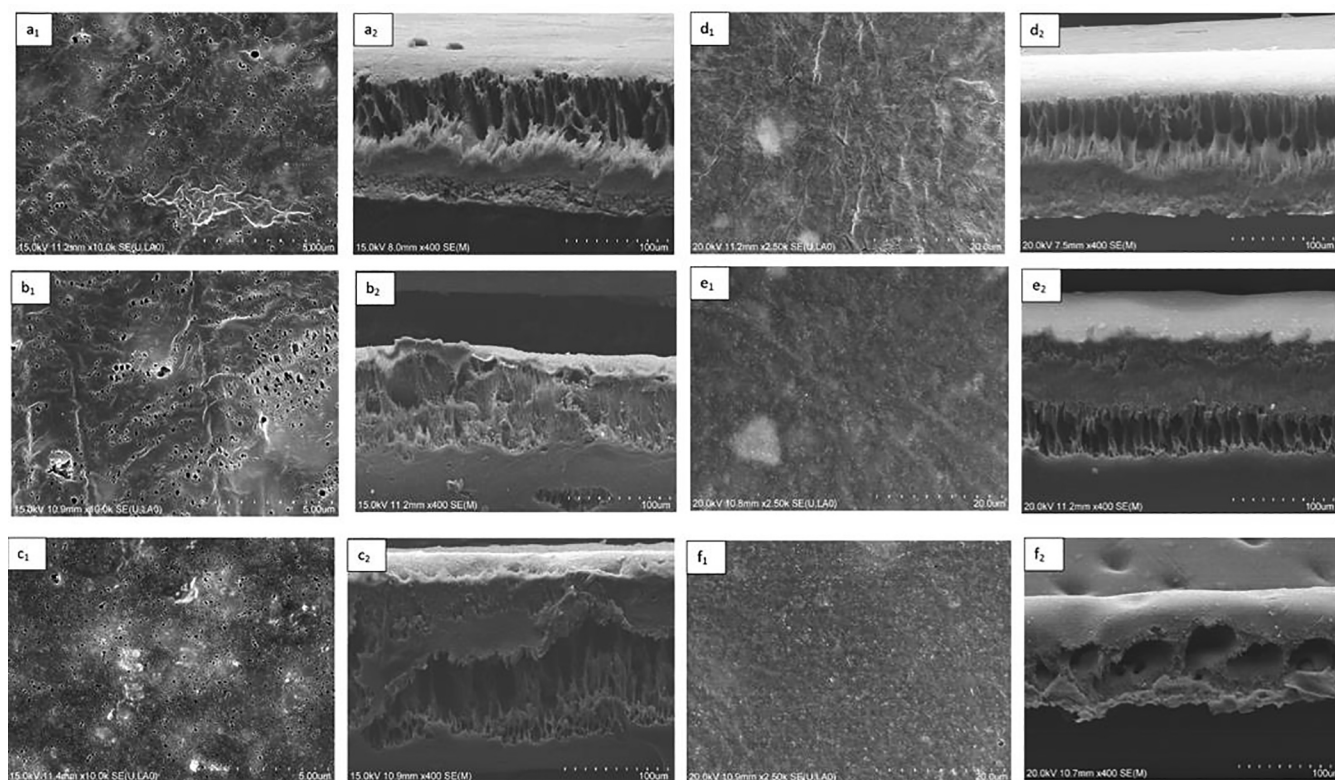


Fig. 2. Surface and cross-sectional of prepared membranes with various ratios of BRM and ZnO. nanoparticles, Subscript1: Surface, Subscript2: cross section (a) PVC-BRM 5%, (b) PVC-BRM 10%, (c) PVC-BRM 15%, (d) PVC-ZnO 5%, (e) PVC-ZnO 10%, (f) PVC-ZnO 15%.

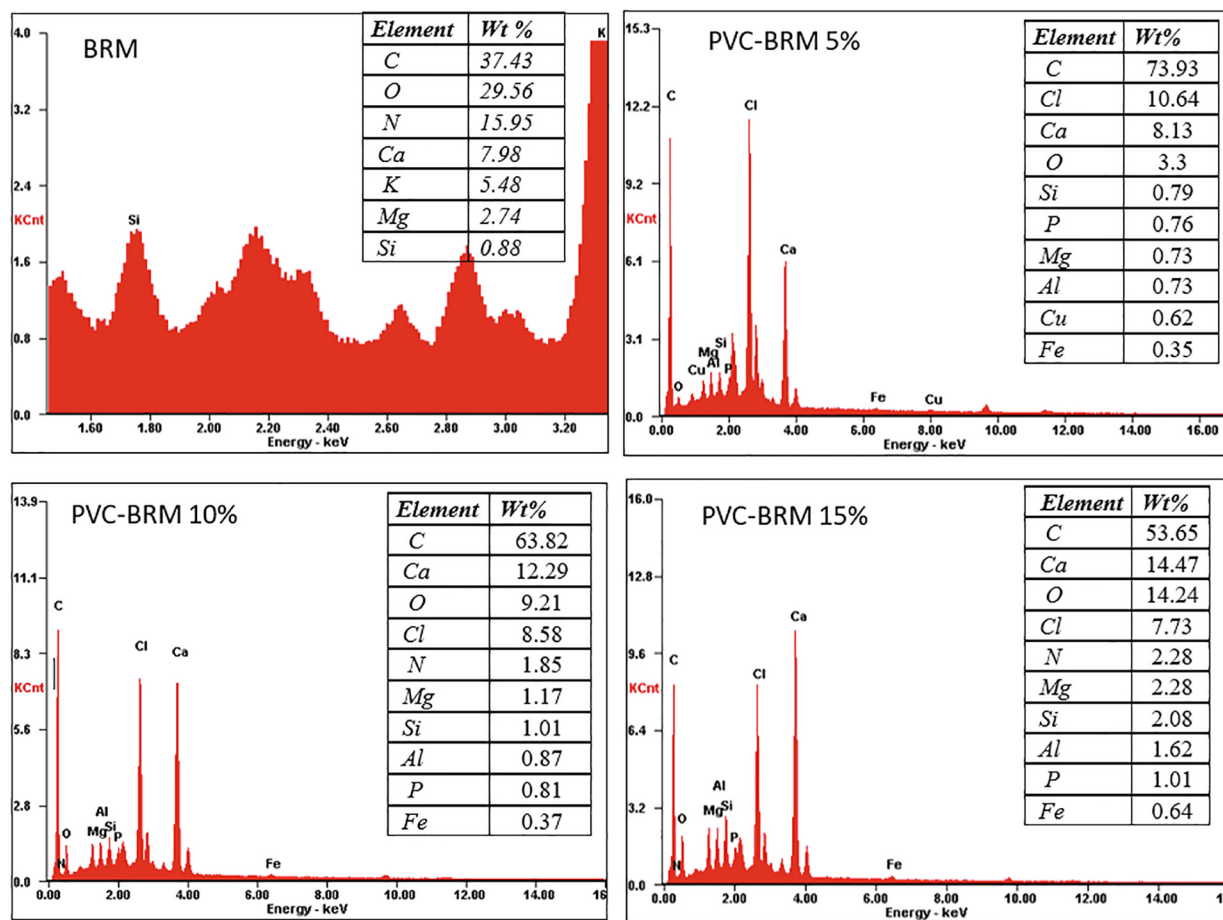


Fig. 3. EDS composition of BRM and PVC-BRM membranes.

in our study in comparison to other modified phosphate selective biochars [38,40,43]. The molar oxygen to carbon (O/C) and [(O + N)/C] ratios are an indication of surface hydrophilicity and polarity, respectively [67,68,69]. The molar O/C ratio of 0.79 and molar [(O + N)/C] of 0.82 in our study show higher value in comparison with other literature [69,70,71], indicate that the surface of BRM is hydrophilic and contains many polar functional groups.

The presence of significant adsorbent elements in the EDS spectra of the PVC-BRM membrane (Fig. 3) and PVC-ZnO membrane (Fig. 4) indicates successful incorporation of adsorbents in the cast MMM. The increase in the adsorbent elements percentage in EDS results corresponds very well with the increase in purging of the incorporated adsorbents in the membranes. For better understanding of the homogeneity of the nanoparticles inside the membrane, EDS maps were taken for both membranes at 15% adsorbent loading, which are presented in Figs. S2 a and b in supplementary data. All EDS maps confirmed that the adsorbents inside the membranes were distributed homogeneously in PVC-BRM and PVC-ZnO 15%.

BET: Texture analysis of the unmodified RM, BRM, and ZnO was performed, and the surface areas (BET) and total pore volumes (V_p) are listed in Table 1. As shown in Table 1, the BET values of the unmodified RM, BRM, and ZnO are 1.40, 8.83, and 13.20 m^2/g , respectively, and the pore values confirm that the samples are in good agreement with a mesoporous structure. Although BRM has a small surface area, it has high phosphate adsorption capacity, which indicates that the phosphate sorption depends on adsorptive interaction with the adsorbed layer more than the adsorbent surface area [72,73].

FTIR: The presence in the FTIR spectra for BRM and ZnO of all the characteristic adsorption bands for phosphate ions demonstrates that adsorption of phosphate ions successfully occurred (Fig. 5). FTIR

measurement for BRM (Fig. 5.a) indicated the presence of the following groups: N–H or ν_2 vibrations of C–O (carboxylic group) (1417 cm^{-1}), C–N stretching (aliphatic amine) (1037 cm^{-1}) and N–H wag (primary and secondary amines) (710 cm^{-1}) [74,75]. A broad band at around $433\text{--}769\text{ cm}^{-1}$ is assigned to the metal–oxygen bending vibration. ν_4 bending vibration of PO_4^{3-} at 562 cm^{-1} and ν_3 stretching PO_4^{3-} vibration in the $1000\text{--}1100\text{ cm}^{-1}$ range were detected after treatment, which confirms phosphate adsorption with metal oxide [76,77]. The bands detected at 870 cm^{-1} (ν_2 vibrations of C–O) are assigned to the CO_3^{2-} group of B-type carbonate apatite. However, this peak indicates the presence of HPO_4^{2-} in the crystal lattice as well [76,78,79,80]. Additionally, the carbonate peaks observed at 1416 cm^{-1} are attributed to the asymmetric stretching of C–O bonds, suggesting the presence of the carboxylic group or likely the incorporation of carbonates into the apatite during treatment [81]. Similar peaks of phosphate adsorption were observed in ZnO nanopowder after phosphate removal (Fig. 5.b). The weak broad peaks apparent around the $2600\text{--}3400\text{ cm}^{-1}$ region might be attributable to O–H stretching and bending vibrations, which would confirm the presence of “free” hydroxyl groups [82] or hydroxyl-bound metal hydroxides. Further, since secondary amines (R_2NH) have only one N–H bond, the peak appears in a single weak band in the $3300\text{--}3000\text{ cm}^{-1}$ region. Tertiary amines (R_3N) are not visible in this region since they do not have an N–H bond [83].

XRD: The X-ray powder diffraction (XRD) patterns for the BRM and ZnO both before and after phosphate adsorption are presented in Fig. 6. The XRD spectra of the BRM showed several peaks (Fig. 6.a), including peaks located at around 2θ , which indicate the amorphous and graphitic nature of the BRM [84] and are in agreement with the elemental composition in the EDS results. Sharp peaks in the BRM pattern indicate different inorganic components [85]. The peaks around 2θ at

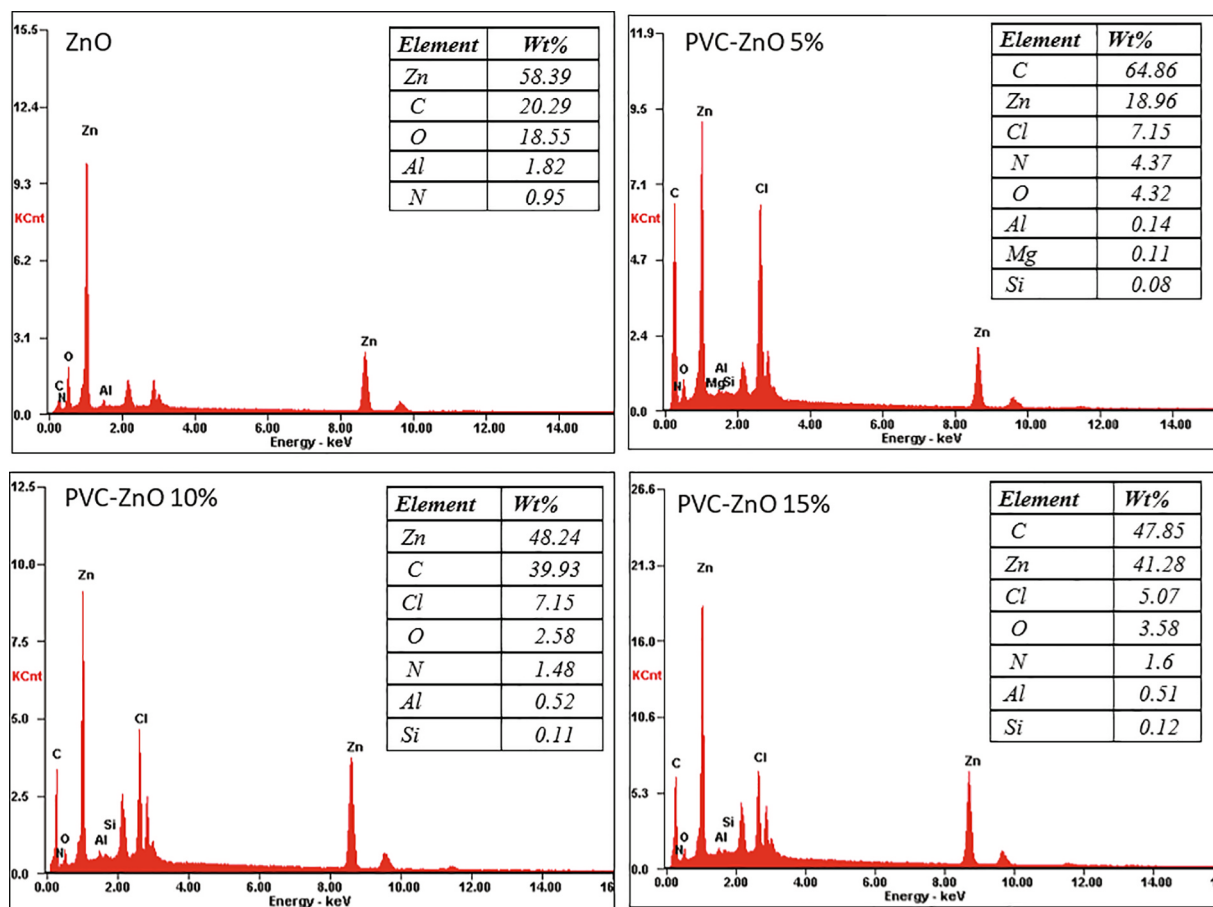


Fig. 4. EDS composition of ZnO and PVC-ZnO membranes.

Table 1

Textural data of RM, BRM, and ZnO.

Sample	BET (m ² /g)	Vp(m ³ /g)	r = Vp/BET (Å)
RM	1.40	0.01	12.85
BRM	8.83	0.01	15.29
ZnO	13.20	0.02	16.73

43°, 62° indicate the presence of MgO in the BRM [86]. Zhang et al. [87] found similar peaks in their experiments with biochar of rice husk; peaks around 2θ at 27°, 29°, and 39° were ascribed to mineral crystals such as SiO₂, CaCO₃, CaSO₄ and Na₄SiO₄ in the biochar. The XRD pattern of BRM after use changed slightly, which suggests successful phosphate adsorption by chemisorption and somewhat physisorption [88]. In contrast, the XRD pattern of ZnO did not change after treatment (Fig. 8.b). As can be seen in Fig. 6.b, the diffraction peaks located at 2θ at 31.6°, 34.2°, 36.08°, 47.4°, 56.4°, 62.7°, 66.3°, 67.9°, 69.02°, 72.5° and 76.9° correlate with diffraction planes (100), (002), (101), (102), (110), (103), (200), (112), (201) and (202), which matches the JCPDS Card No. 36-1451, demonstrating the wurtzite structure of the ZnO [89]. A similar finding has also been reported in other research [83,90,91,92,93,94,95]. No additional peaks confirm the chemical purity, and the sharp narrow peaks indicate that both BRM and ZnO were well crystallized.

XPS: The XPS results (Fig. 7) for elemental composition and valence state are consistent with those of the XRD and the EDS analyses, which confirm the successful sorption of phosphate on the membranes. A P 2p peak with binding energy about 133.6 eV was observed for phosphate-loaded in both PVC-BRM and PVC-ZnO (Fig. 7.a), which confirms the successful adsorption of phosphate on the membranes [77]. However,

determination of phosphate and N-functional groups is not easy due to the high bond energy of the carbon and Cl⁻ peaks and their repulsion, thus resulting in some deviation [96]. In Fig. 7.b, C and O are determined as the most common component of BRM, which is in agreement with the EDS and FTIR results. However, some carbon peaks attributed to the PVC structure have similar peaks in the XRD patterns of both membranes [97]. Zn, O, and C peaks were detected as the most common component of ZnO nanopowder (Fig. 7.c), which is in agreement with EDS data (Fig. 4). Two fitting peaks situated at about 1045.5 and 1022.4 eV are attributed to Zn 2p_{1/2} and Zn 2p_{3/2}, respectively. Similar Zn peaks were observed in [77,98,99,100]. The increase in the intensity of the peaks confirms the successful adsorption of phosphate. The emergence of all of the characteristic adsorption bands for phosphate ions within the FTIR, XPS and XRD spectra of BRM and ZnO in either the adsorbent or membrane shows that successful adsorption of phosphate ions occurred.

3.2. Adsorption experiments

3.2.1. Kinetic studies

A kinetic study was undertaken to determine the mechanism and rate of the adsorption reaction [101]. Two kinetic models were applied in analysis of the sorption data of phosphate onto adsorbents: a pseudo-first-order model and a pseudo-second-order model (see Table S1 for details) [77]. The linearized form of these models for BRM and ZnO as a function of time is depicted in Figs. S3. a - d in supplementary data. The kinetic parameters and coefficients are shown in Table 2. The highest value of the correlation coefficients of the R² parameters revealed that all kinetic results for phosphate exhibit a better fit with the pseudo-second-order model, indicating that multiple mechanisms controlled

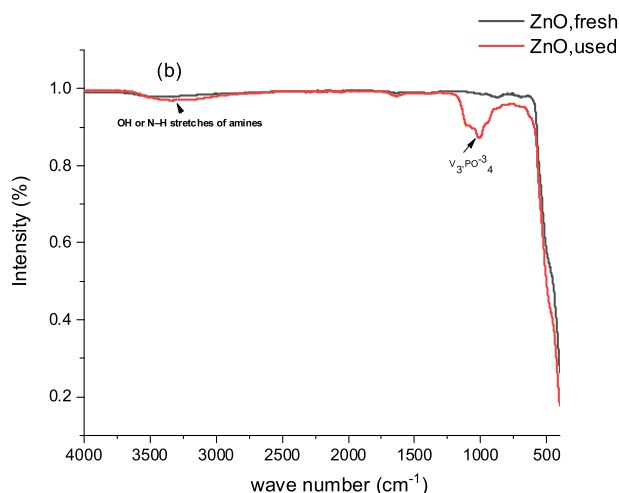
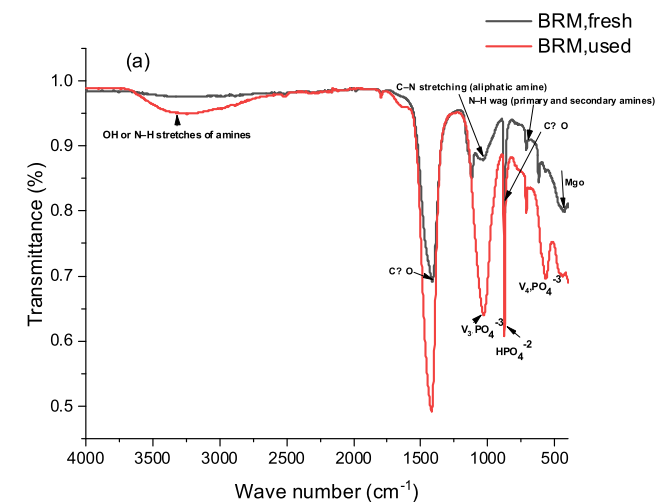


Fig. 5. FTIR spectra of adsorbent before and after phosphate adsorption (a) BRM (b) ZnO.

the adsorption of phosphate on both the BRM and ZnO samples [42]. Furthermore, chemisorption is the dominant rate-controlling mechanism during mass transfer between the sorbate and sorbent [102,103,104]. The theoretical values (q_e, cal) of adsorption capacities are in good agreement with those of the experimental values (q_e, exp) (Table 2) obtained from the pseudo-second-order kinetic model for both

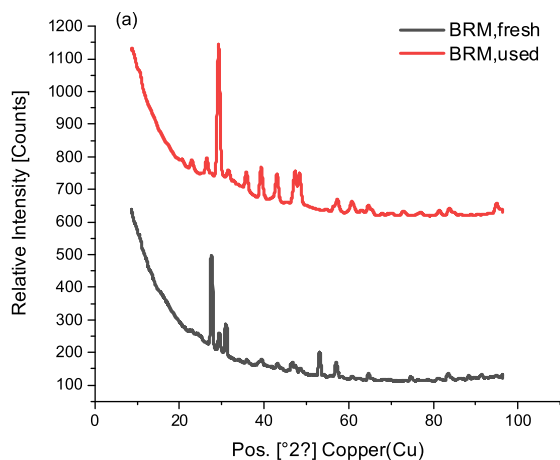


Fig. 6. XRD pattern of adsorbents before and after phosphate adsorption (a) BRM (b) ZnO.

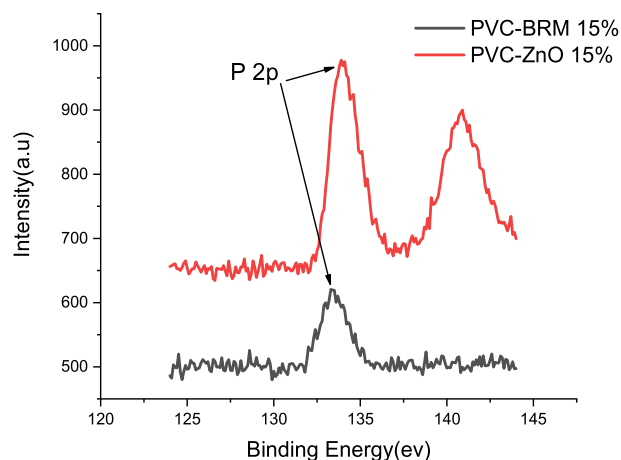


Fig. 7. a. Phosphate peak in XPS of PVC-BRM and PVC-ZnO 15% after phosphate adsorption. b. XPS pattern of PVC-BRM 15% before and after phosphate adsorption. c. XPS pattern of PVC-ZnO 15% before and after phosphate adsorption.

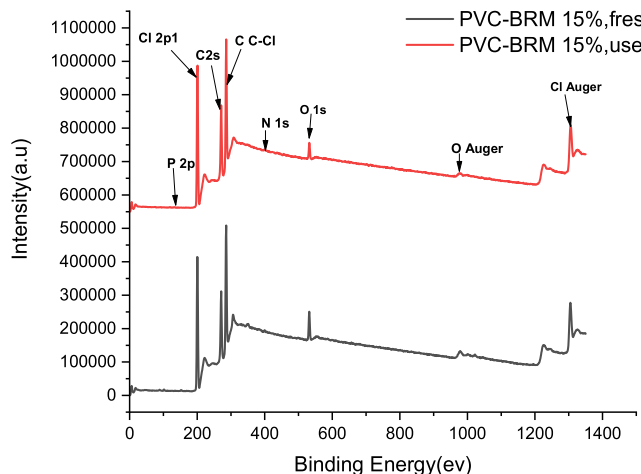


Fig. 7. (continued)

BRM and ZnO. The pseudo-second-order kinetics have been reported in many studies [57,74,75,77,102,105,106,107,108,109,110,111]. It can be seen from the graphs and table that BRM showed higher adsorption capacity than ZnO in all of the PO_4^{3-} concentration solutions.

As seen in Fig. S3 and Table 2, the adsorption capacity increased with increasing initial phosphate level, and both adsorbents exhibited

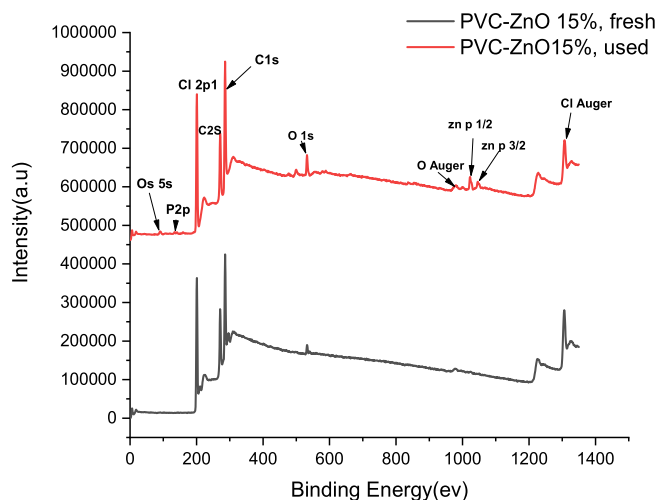


Fig. 7. (continued)

high adsorption capacity toward phosphate under optimum conditions. The data shows that when the initial phosphate concentration was 160 mg/L PO_4^{3-} , the maximum adsorption capacity was 49.20 mg/g and 26.47 mg/g for BRM and ZnO, respectively. This increased adsorption capacity may be because higher concentrations of phosphate provide the driving force to improve mass transfer between the aqueous and solid surface and better filling of adsorption sites [66,112]. These data also demonstrate the potential applicability of BRM adsorption from low to high levels of phosphate in wastewater. The kinetic curve for the studied phosphate ion showed that the adsorption was initially rapid for BRM adsorbent; more than 80% of phosphate removal occurred within 5 min in a solution of 40 mg/L PO_4^{3-} , which makes the adsorption economical in practice. At the initial adsorption stage, the surface of all adsorbents contains many available active sites for phosphate binding, and fast adsorption took place. However, the removal efficiency decreased with increased initial phosphate concentration in both isotherm and kinetics experiments since fewer active adsorption sites were available at higher initial PO_4^{3-} -P concentrations [66]. Maximum adsorption capacity increased over time until it reached 32.64, 40.72 and 49.20 mg/g for 40, 80 and 160 mg/L PO_4^{3-} in 45 min contact time in BRM (Fig. S3.b). The same trend was observed in phosphate removal by ZnO nano-adsorbent in our study (Fig. S3.d) and has also been seen in other studies [102,107].

3.2.2. Isotherm studies

The Langmuir, Freundlich and Temkin isotherm models were used for modeling of phosphate adsorption. Fitting plots are shown in Fig. S4 in supplementary data. The calculated isotherm parameters and respective R^2 values of the adsorption isotherm are presented in Table 3. Phosphate adsorption by BRM is illustrated better by the Langmuir model with R^2 values of 0.999 and smaller chi-square than by the other models, which is in agreement with other studies [66,111,113,114,115]. However, the Freundlich model interpreted the adsorption process well at higher temperatures, suggesting that the

Table 2
Coefficients of sorption kinetics for BRM and ZnO.

Adsorbent	Initial concentration(mg/L)	qe experimental (mg/g)	First order			Second order		
			qe	k_1	R^2	qe	k_2	R^2
BRM	40	32.64	29.99	0.31	0.96	33.23	0.01	0.96
	80	40.72	36.17	0.29	0.93	40.73	0.09	0.95
	160	49.20	42.29	0.45	0.93	45.96	0.01	0.95
ZnO	40	10.49	9.81	0.52	0.98	10.31	0.10	0.99
	80	17.12	14.92	0.28	0.92	16.63	0.02	0.97
	160	26.47	23.64	0.24	0.94	26.46	0.01	0.97

Table 3

Temkin, Freundlich and Langmuir isotherms constants for the adsorption of phosphate onto BRM and ZnO.

Adsorbent	Isotherm model	Isotherm parameters	Temperature (K)		
			298	308	318
BRM	Langmuir	Q_0	50.47	53.97	65.41
		b	0.19	0.25	0.95
		R_L	0.06	0.05	0.01
	Freundlich	R^2	0.99	0.99	0.87
		k_F	20.91	24.1	27.71
		n	5.392	5.73	4.37
	Temkin	R^2	0.99	0.98	0.96
		A_T	7.37	12.14	24.29
		b	333.62	338.43	282.29
ZnO	Langmuir	R^2	0.99	0.99	0.93
		Q_0	35.95	37.73	38.76
		b	0.01	0.02	0.05
	Freundlich	R_L	0.34	0.35	0.37
		R^2	0.99	0.99	0.99
		k_F	2.58	5.59	11
	Temkin	n	2.11	2.99	4.3
		R^2	0.99	0.98	0.98
		A_T	0.11	0.26	1.15
	b	564.36	447.67	344.7	
	R^2	0.99	0.98	0.98	

adsorption is controlled by multiple processes [75,116]. Similarly, the Langmuir isotherm was fitted better for ZnO with R^2 values of 0.99 and lesser chi-square. The fitting of experimental data depends not only on the adsorbent but also on the adsorbate. Further, adsorption capacity values for an adsorbent depend on experimental conditions, such as pH, adsorbate concentration, ionic strength, temperature, and coexisting chemical species in the solution [117].

From Fig S4, it can be seen that removal efficiency and q_e values increase with increasing solution temperature for both BRM and ZnO, indicating that the reaction is endothermic and is enhanced at higher temperatures. With increasing temperature, the desired intermolecular forces between the adsorbate and adsorbent are much stronger than between the adsorbate and solvent [118]. As a result of the chemical interaction, the reactivity of the surface sites and the rate of intraparticle diffusion of sorbate ions into the pores of the adsorbent increase at higher temperatures [75,106,119]. The endothermic nature of the phosphate adsorption has been reported also by other researchers [39,118,120,121]. In addition to the Langmuir isotherm, the adsorption process can be defined in terms of separation factor (RL) (Table S1). If ($RL = 0$), then the process is irreversible. If ($0 < RL < 1$), then the process is favorable. If ($RL = 1$), then the curve obtained is linear. If (RL greater than 1), then the process is unfavorable [122]. According to Table 3, the RL values in this study were between 0 and 1 for both adsorbates, indicating that the adsorption process is favorable [107].

The values of n in the Freundlich isotherm are in the range of 2–10 and represent good adsorption, which is in agreement with the BRM value of about n:5 [123]. Moreover, in the Temkin isotherm model (Table 3), the b values are higher than 80 kJ/mol, indicating a chemical adsorption process, and there is consequently strong ionic interaction between the phosphate and adsorbent [75]. The adsorption capacity of

BRM and ZnO, as calculated by the Langmuir equation, is approximately 50.47 and 35.95 mg/g in T:298 K (25 °C), respectively, which suggests that the BRM has high phosphate adsorption capacity.

Here, we evaluated the adsorption performance of BRM in different initial phosphate concentration and compared it with the performance of other adsorbent materials reported in Table S2. As can be seen the high removal efficiency of 99.7% and adsorption uptake of 78.24 mg/g in T:318 K (45 °C) are comparable with other studies. However, comparing the adsorption capacities of adsorbents performed in different experimental conditions could not represent correct perceptions [58]. Thus it is necessary to evaluate the effectiveness of different adsorbents with a more practical index. Therefore, the partition coefficient (PC) was used here as a practical indicator to determine the efficiency of sorbents. The partition coefficient can be defined as the ratio of adsorbate concentration on the adsorbent solid phase to the adsorbate concentration in the liquid phase [59]. The PC value of 31.92 mg/g/μM for BRM in 40 mg/L PO_4^{3-} is significantly comparable with other studies. Decreasing the PC with increasing the phosphate concentration represents better removal efficiency in a lower concentration.

3.2.3. Effect of pH

The effect of solution pH on phosphate adsorption by the BRM samples is shown in Fig. 8. The other main anions and cations were also analyzed to investigate possible mechanisms. Several types of

phosphorus (H_3PO_4 , H_2PO_4^- , HPO_4^{2-} and PO_4^{3-}) can be present in the solution depending on the pH (see Fig. 8.a). It can be seen that the optimal solution pH for BRM was 3.0, and the adsorption efficiency for phosphate recovery decreased with an increase in solution pH. This trend is in agreement with Li et al. [124], Xu et al. [125] and Bacelo et al. [117] study, while in other studies increasing pH improved the removal efficiency due to the formation of calcium phosphate [1,106]. The lower adsorption free energy of H_2PO_4^- at acidic pH in comparison to HPO_4^{2-} at basic pH might be the reason for better adsorption at acidic pH [126]. Moreover, the adsorbent surface is protonated and becomes more positive by lowering the pH of the solution, thus significantly absorbing more negatively charged phosphate anions [126,127,128]. Phosphate adsorption capacity decreased at high pH values because the hydroxide ions dominated the phosphate species, and they compete for the consumption of adsorption sites [106,128,129,130]. Also, higher pH causes the adsorbent surface to carry more negative charges that significantly repel the negatively charged ions in the solution [106]. We found a remarkable agreement between the removal efficiency with the Zeta potential for the different pH (Fig. 8.b). The reduction of the negative charge at acidic pH was observed in zeta potential measurements, which confirmed the reduction of electrostatic repulsion between the BRM and the anion. The same trend has been reported by [131,132,133,134]. Furthermore, alkaline conditions increase the deprotonation degree of oxygen-containing functional groups, resulting in

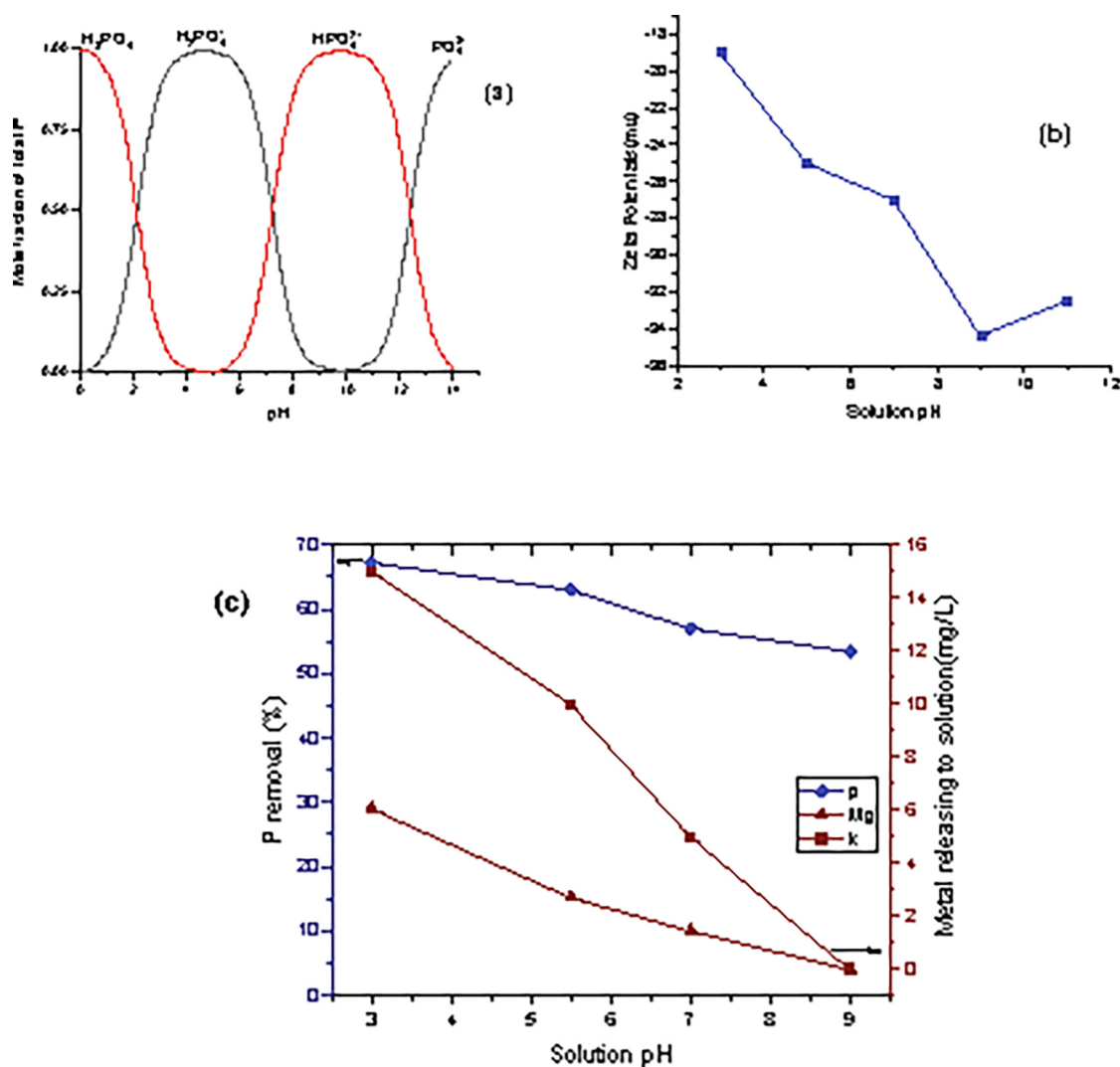


Fig. 8. Effect of pH on (a) phosphate components, (b) Zeta potential of BRM, (c) phosphate removal, and related metal releasing using feed concentration of 80 mg/L PO_4^{3-} .

a decrease in zeta potential [131]. Moreover, the concentration of dissolved K^+ and Mg^{2+} decreased when the initial pH value increased (Fig. 8.b), which causes inhibition of K^+ and $MgPO_4$ precipitation and hence reduces P adsorption [1]. In this experiment, no heavy metal leaching from BRM was observed at different pH, indicating that the usage of biochar is safe from the environmental perspective.

3.3. Filtration experiments

3.3.1. Effect of different adsorbent loading on structural properties and phosphate removal efficiency of the membranes

PVC-BRM and PVC-ZnO membranes were prepared with three different loading amounts of BRM and ZnO respectively. The composition of the polymeric membrane solutions is shown in Table S3 in supplementary data. The characterization test results of the fabricated MMMs are presented in Table S4. The mean pore size of all the membranes (calculation base on Eq. (3) in Text S1) are in the range of 20–30 nm, which means that our membranes are MF-type membranes. As BRM and ZnO nanoparticle loadings increased from 5 to 15 wt%, the average pore size increased from 19.8 nm to 28.2 nm for the PVC-BRM membrane and from 20 to 30 nm for the PVC-ZnO membrane, respectively. The pore size is possibly dependent on the viscosity of the polymer solution, loading amount and characteristics of the adsorbent as a filler [44,135]. Subsequently, the increase in adsorbents loading resulted in an increase in membrane water flux, which may be attributed to different causes, for example, increased number of pores and higher surface roughness [136] in addition to larger pores. Reduced contact angle was observed with an increase in loading of the adsorbents, due to the hydrophilic characteristic of BRM and ZnO, which is in agreement with the EDS elemental composition results that the molar oxygen to carbon (O/C) showed the hydrophilicity of BRM. The performance of the MMMs as regards separation of phosphate ions was investigated at a feed concentration of 80 mg/L in Fig. 9.a & b, respectively. It can be seen that the membranes exhibited the highest removal efficiency for phosphate ions for both the PVC-BRM MMM and PVC-ZnO MMM at adsorbents loading of 15 wt%. This finding might be attributed to the ions being able to transport through the membrane more easily, because greater adsorbents content could provide more channels for ion transport, thus reducing ion transmembrane resistance [137]. The PVC-BRM membranes showed higher phosphate removal efficiency than the PVC-ZnO membranes at all adsorbent loadings: for example, PVC-BRM membranes at 5%, 10% and 15% loading showed about 23.97%, 18.75% and 49.77% (Fig. 9.a) higher removal of phosphate compared to the corresponding PVC-ZnO membranes respectively at 5 min contact time (Fig. 9.b).

3.3.2. Effect of initial phosphate concentration

The effect of feed concentration on phosphate removal efficiency was investigated using PVC-BRM-15% and PVC-ZnO-15% membranes as these membranes had the highest removal efficiency. For this experiment, feed solutions were prepared at concentrations of 40, 80 and 160 mg/L PO_4^{3-} . Fig. 10.a & b display the removal efficiencies for the phosphate ions versus time at different phosphate concentrations by PVC-BRM-15% and PVC-ZnO-15%, respectively.

As can be seen in Fig. 10.a, the removal efficiency at the beginning of the experiments is high, as the membrane is fresh and contains numerous active sites. The phosphate removal efficiency of the PVC-BRM-15% MMM after 1 min of contact time was measured as about 100%, 99.7% and 99.7% at feed concentration of 40, 80 and 160 mg/L, respectively. The values for the PVC-ZnO-15% MMM after 1 min of contact time were about 59.6%, 54.2% and 22% for 40, 80 and 160 mg/L PO_4^{3-} concentration, respectively (Fig. 10.b). However, phosphate removal efficiency decreased over time as it reached to 55%, 46% and 29% for PVC-BRM-15% MMM at feed concentration of 40, 80 and 160 mg/L and 30 min contact time, respectively. In comparison, this value was 36%, 32% and 20% for PVC-ZnO-15% MMM, respectively, in

the same condition. Thus, similar to the kinetic study in adsorption experiments (subsection 3.2.1), lower feed concentration of phosphate showed better removal efficiency, and increasing phosphate ion levels lowered the removal efficiency in both the PVC-BRM and PVC-ZnO membranes.

However, reducing the removal efficiency between 40 and 80 mg/L PO_4^{3-} was not significant as a higher phosphate concentration might cause a higher concentration gradient that provides a strong driving force to maintain the adsorption rate capacity [138]. Also, this phenomenon showed that similarly to the BRM, the corresponding membrane (PVC-BRM-15% MMM) also has a great performance for the removal of phosphate in a wide range of pollutant concentrations. Nevertheless, removal efficiency decreased significantly for 160 mg/L PO_4^{3-} due to faster saturation of reaction sites on the membrane [66,139].

Furthermore, saturation time for the PVC-BRM membrane was longer than for PVC-ZnO membrane, and even after 60 min, the PVC-BRM membrane did not reach to saturation point. It can be concluded that the removal process of PO_4^{3-} ions using a PVC-BRM MMM possess rapid kinetics compared to a PVC-ZnO MMM. We did not observe anions leaching in the membranes in comparison to batch adsorption study.

3.4. Selective phosphate recovery from multi-component solution by adsorbents and membranes

Municipal effluent typically contains other anions that could influence the removal of phosphate ions. The ions taken into account in this study are sulfate, nitrate and chloride, of which 1 mM concentration of each (about 80 mg/L SO_4^{2-} , 58 mg/L NO_3^- , 30 mg/L Cl^- and 78 mg/L PO_4^{3-}) were investigated for both the adsorbents and membranes, presented in Fig. 11.a-c. It was found that the presence of other ions does not affect the removal efficiency of PO_4^{3-} onto BRM and ZnO adsorbents (Fig. 11.a). However, the presence of the ions caused a slight decrease in the efficiency of phosphate removal by the PVC-BRM 15% membrane. The removal efficiency of the PVC-BRM membrane (Fig. 11.b) in the absence of interfering ions was 48%, 35% and 32% in 30 to 60 min, respectively (Fig. 10.a, 80 mg/L). In comparison, the removal efficiency for phosphates was reduced to 36%, 21% and 19% in 30 to 60 min, respectively, in the presence of interfering anions. Jia et al. [140] observed decreasing phosphate removal efficiency in the presence of other anions. The most competitive anion was SO_4^{2-} . One possible

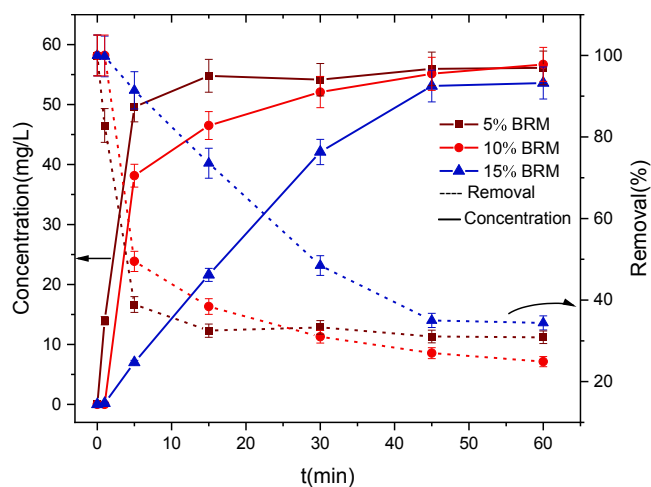


Fig. 9. a. Effect of adsorption loading on removal efficiency and concentration changes of phosphate versus time using PVC-BRM membrane and feed concentration of 80 mg/L PO_4^{3-} . b. Effect of adsorption loading on removal efficiency and concentration changes of phosphate versus time using PVC-ZnO membrane and feed concentration of 80 mg/L PO_4^{3-} .

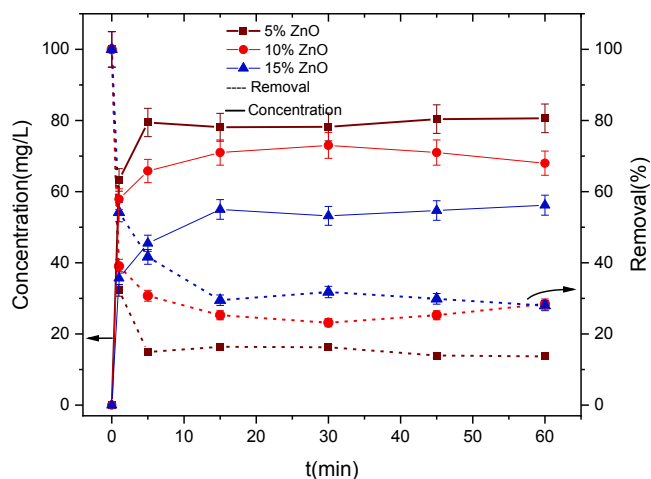


Fig. 9. (continued)

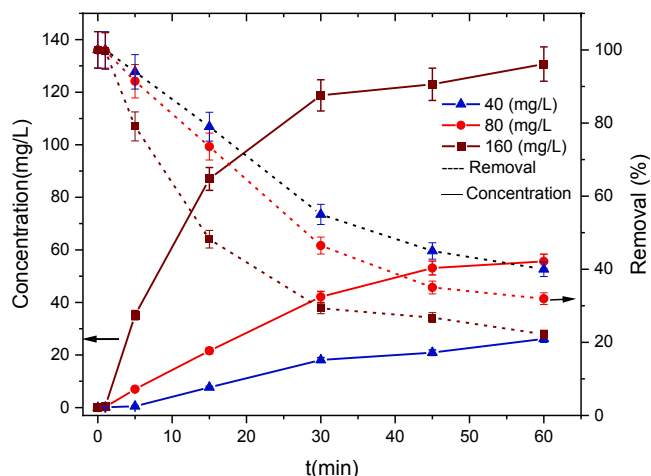


Fig. 10. a. Effect of initial phosphate concentration on removal efficiency and concentration changes versus time using PVC-BRM 15% membrane and feed concentration of 80 mg/L PO_4^{3-} . b. Effect of initial phosphate concentration on removal efficiency and concentration changes versus time using PVC-ZnO 15% membrane and feed concentration of 80 mg/L PO_4^{3-} .

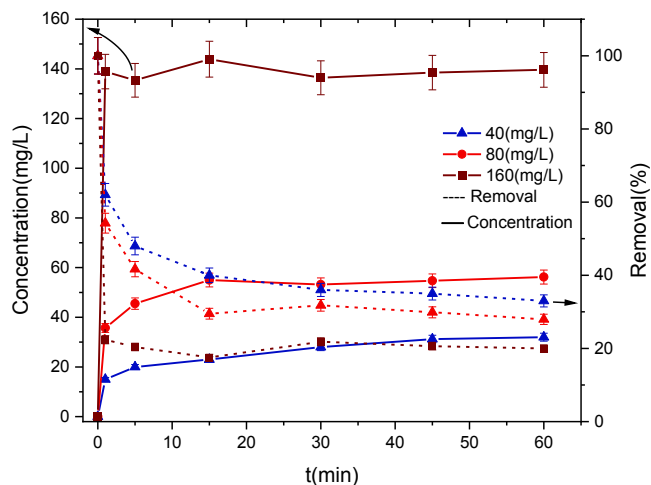


Fig. 10. (continued)

explanation is that hydration size and the charge of coexisting ions might account for this order [141]. Another possibility is that the fixed ion-exchange sites typically have superior attraction forces for

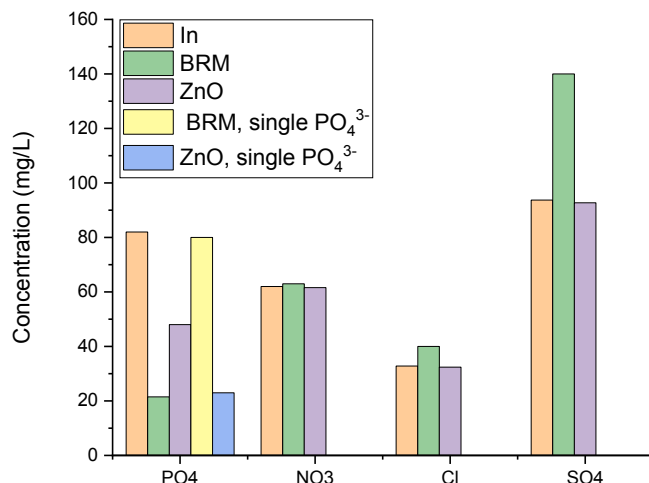


Fig. 11. a. Effect of multi-component feed solution on phosphate removal using BRM/ZnO absorbents. b. Effect of multi-component (PO_4^{3-} , SO_4^{2-} , NO_3^- and Cl^-) on removal efficiency and concentration changes of phosphate versus time using PVC-BRM 15% membrane. c. Effect of multi-component (PO_4^{3-} , SO_4^{2-} , NO_3^- and Cl^-) on removal efficiency and concentration changes of phosphate versus time using PVC-ZnO 15% membrane.

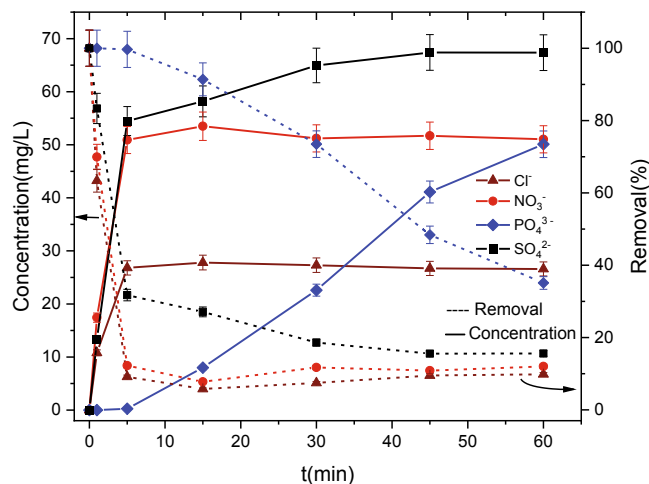


Fig. 11. (continued)

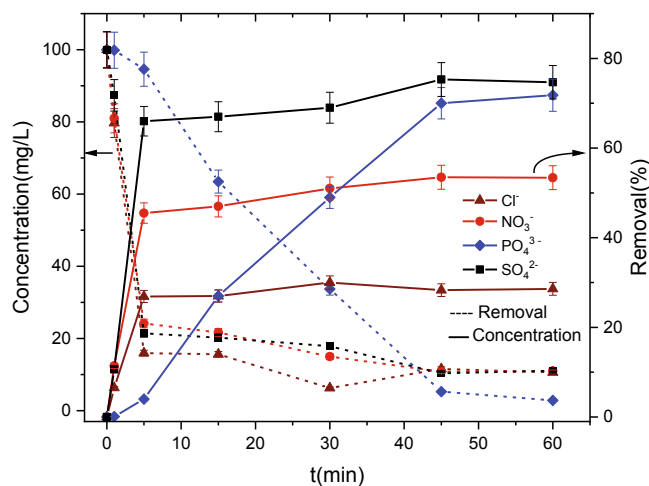


Fig. 11. (continued)

multivalent counter-ions than monovalent ions [142]. The valence of PO_4^{3-} and SO_4^{2-} is -3 and -2 , respectively. However, the molar mass of SO_4^{2-} is 96, that of PO_4^{3-} is 94.97, NO_3^- has molar mass of 62.0 and Cl^- 35.45 g/mol. Hence, with longer contact time, SO_4^{2-} affects PO_4^{3-} removal to a greater extent than the other anions. Similarly, even though both NO_3^- and Cl^- have negative charge, the molar mass of NO_3^- is higher than Cl^- [141]. Likewise, as can be seen in Fig. 11.c, the presence of competitive anions showed negligible effects on the removal of phosphate by PVC- ZnO 15%.

3.5. Application of BRM in phosphate removal and recovery from different wastewaters

Real wastewater conditions differ from synthetic solutions because of the diverse composition of anions and cations, color, soluble solids, and total organic components found in real wastewaters. Hence, the actual behavior and efficiency of adsorbents in real wastewater effluent needs to be studied. In this work, a number of real water samples were investigated (Table 4). The municipal wastewater samples were prepared from secondary clarifier of a conventional activated sludge system at the Mikkeli wastewater treatment plant in Finland. In the first condition, we used wastewater without phosphate spike, and in the second condition, we spiked phosphate to increase its concentration. Additionally, agricultural runoff samples were prepared by mixing 10 g of garden soil with 100 mL water agitated for 1 h. As can be seen in Table 4, all phosphate was removed, indicating that BRM could be a promising engineered adsorbent for efficient phosphate removal from different wastewaters before discharge to water bodies.

3.6. Desorption and reusability studies of BRM and the PVC-BRM membrane

Desorption of phosphate from loaded BRM particles by different solutions (NaCl 1 M, NaCl 3 M and NaOH 3 M) was evaluated. It was found that NaCl 1 M did not affect phosphate recovery and regeneration of BRM, whereas 35% and 44% phosphates were released in NaCl 3 M and NaOH 3 M, respectively. Furthermore, 50% and 75% phosphate adsorption were found in the second cycle. The generally low phosphate desorption rates for NaCl suggest strong interaction between adsorbate and adsorbent or they may be a result of inadequate extracting solution and reaction time [40,66,143]. It also suggests that phosphate adsorption is more a result of chemical adsorption than physical adsorption. Moreover, these results show that BRM can be used as a slow-release fertilizer as it does not have the fast nutrient leaching issues found with other fertilizers. The lower sorption ability of regenerated biochar than fresh BRM could be because of a permanent adsorption reaction in the active site of the biochar or lost porosity owing to precipitated compounds [144]. 32% and 5% of the phosphate was recovered from BRM and ZNO membranes by 1 M NaCl. However, regenerated PVC-BRM 15% showed almost the same removal efficiency as the fresh membrane (Fig. 12.a). The improved removal efficiency of the ZnO membrane after regeneration suggests that the functional groups in ZnO might be activated by NaCl (Fig. 12.b). In the case of the PVC-BRM membrane, replacement of adsorbed phosphate by the Cl^- ion might be occurring due to the greater surface area of adsorbent on the

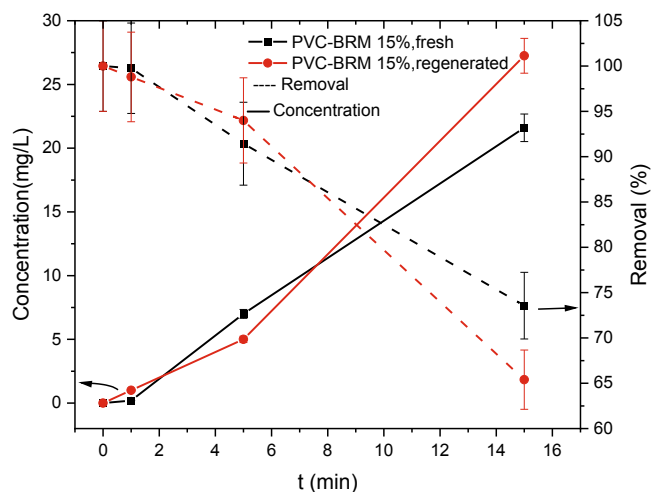


Fig. 12. a. The removal efficiency and concentration changes of phosphate versus time using regenerated PVC-BRM 15% membrane in feed concentration of 80 mg/L PO_4^{3-} . b. The removal efficiency and concentration changes of phosphate versus time using regenerated PVC-ZnO 15% membrane in feed concentration of 80 mg/L PO_4^{3-} .

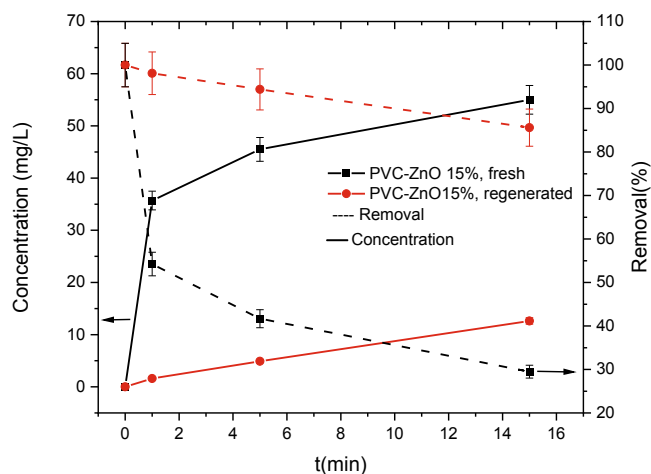


Fig. 12. (continued)

membrane or due to different phosphate adsorption mechanisms in the membrane. The high regeneration rate of the membranes shows that they could be reused for several cycles of PO_4^{3-} removal.

3.7. Possible reaction mechanisms for phosphate sorption by BRM

Surface area: Although the BET results in our study did not show a high surface area for biochar, high phosphate uptake capacity was observed. These results suggest that physisorption on the surface area of BRM is not the important factor affecting phosphate uptake capacity. Several other studies have concluded that P uptake is not only dependent on the surface area of biochar [37,66,129,145,146].

Table 4
Application of BRM on different wastewater.

Water component		PO_4^{3-} (mg/L)	NO_3^- (mg/L)	Cl^- (mg/L)	SO_4^{2-} (mg/L)
Secondary clarifier (1)	Before treatment	1.28	115.81	71.00	127.13
	After treatment	0.00	114.80	80.80	172.08
Secondary clarifier (2)	Before treatment	20.25	115.82	71.00	127.13
	After treatment	0.00	116.08	82.10	180.14
Agricultural runoff	Before treatment	9.00	55.62	38.13	282.52
	After treatment	0.00	55.00	45.03	310.11

Surface charge and functional group: The different functional groups of carboxylic, aliphatic amine, primary and secondary amines and “free” hydroxyl groups were observed in the FTIR results for the biochar. However, the negative charge of our biochar (Zeta potential measurement) suggests that the positive functional group would be less effective for absorbing opposite charge ions such as phosphate. Other studies have also proposed such an opinion [66,147]. The better phosphate removal at acidic pH (subsection 3.3.2.) might be due to higher positive charge in this pH. However, higher pH causes repulsion of the negatively charged solute in the solution and increases competition between OH and PO_4^{3-} for consumption of adsorption sites. Study of the effect of the multi-component solution on BRM (subsection 3.3.4.) showed that cations were not removed by the biochar, which indicates that functional group adsorption had little effect on the cation.

Anion exchange: The FTIR results showed evidence of adsorption of phosphate onto the surface of functional groups in the P-loaded biochar in our study. Further, the results showed release of Cl^- , OH^- , and SO_4^{2-} from biochar to the solution, which might represent phosphate replacement with these anions, which act as mobile ions connected to cationic functional groups in the BRM. However, the amount of anion release did not change with time and all anion release occurred in the first 15 min, and the removal percentage was high even in basic pH, so other mechanisms should be involved as well, and ion exchange might be more effective at the beginning of the adsorption period.

Metal oxides: Many studies have shown a positive correlation between PO_4^{3-} -P adsorption and several types of metallic ions (Ca^{2+} , Mg^{2+} , Fe^{3+} , Al^{3+} , La^{3+} , K^+ , etc.) present in biochar, mainly if the metals are presented as basic functional groups [[37,65,66,148,129,117]]. The metal oxide surface becomes hydroxylated in contact with water and thus introduces either a positive or negative surface charge depending on the solution pH [149]. EDS mapping showed the presence of metal ions in the biochar and metal release (K^+ , Mg^{2+} , Ca^{2+} , Si^{4+}) into the solution was also observed in

our experiments. The peaks around 500 cm^{-1} in the FTIR spectra represent Mg-O and weak broad peaks apparent around the $3400\text{--}2600\text{ cm}^{-1}$ region might be attributed to hydroxyl and belongs to metal hydroxide. Additionally, the XRD spectra of the biochar showed several peaks that were likely attributable to SiO_2 , CaO , and MgO [85]. The peaks around 2θ at 42° , 62° indicated the presence of MgO in the biochar. Possible mechanisms of phosphate adsorption on metal oxide and hydroxides involve surface precipitation of metal-phosphate, electrostatic attraction, ligand exchange forming covalent bonds between phosphate and the metal cation (inner-sphere surface complexation), which were then deposited on the surface of the biochar, and hydrogen bonding between H and O from phosphate and metal oxides [66,117,129,146]. On the other hand, these metal elements that are partly released from biochar into the solution will react with phosphates and produce precipitation or bonding with hydrogen and phosphate [146]. No metal ion release to the solution in the membranes shows that that phosphate adsorption onto the adsorbent might not be caused by chemical precipitation but rather by chemical adsorption through exchange with OH on the hydroxylation surface of the ZnO [92]. Fig. 13 shows schematic diagrams of major sorption mechanisms of phosphate for the biochar used in our study.

4. Conclusion

Biochar from *Rosmarinus officinalis* leaves (BRM) was fabricated using pyrolysis of *Rosmarinus officinalis* leaves (RM) in a simple and environmentally friendly preparation method. The high adsorption capacities of BRM make it a promising material for the removal of phosphate. Incorporation of BRM in a membrane matrix expands the range of possible applications for BRM and resolves the challenges of use of a single adsorbent in wastewater treatment systems. The BRM showed high adsorption capacities for phosphate in single and multi-component systems as well as in different wastewaters. In the membrane, the efficiency decreased slightly in the presence of other anions,

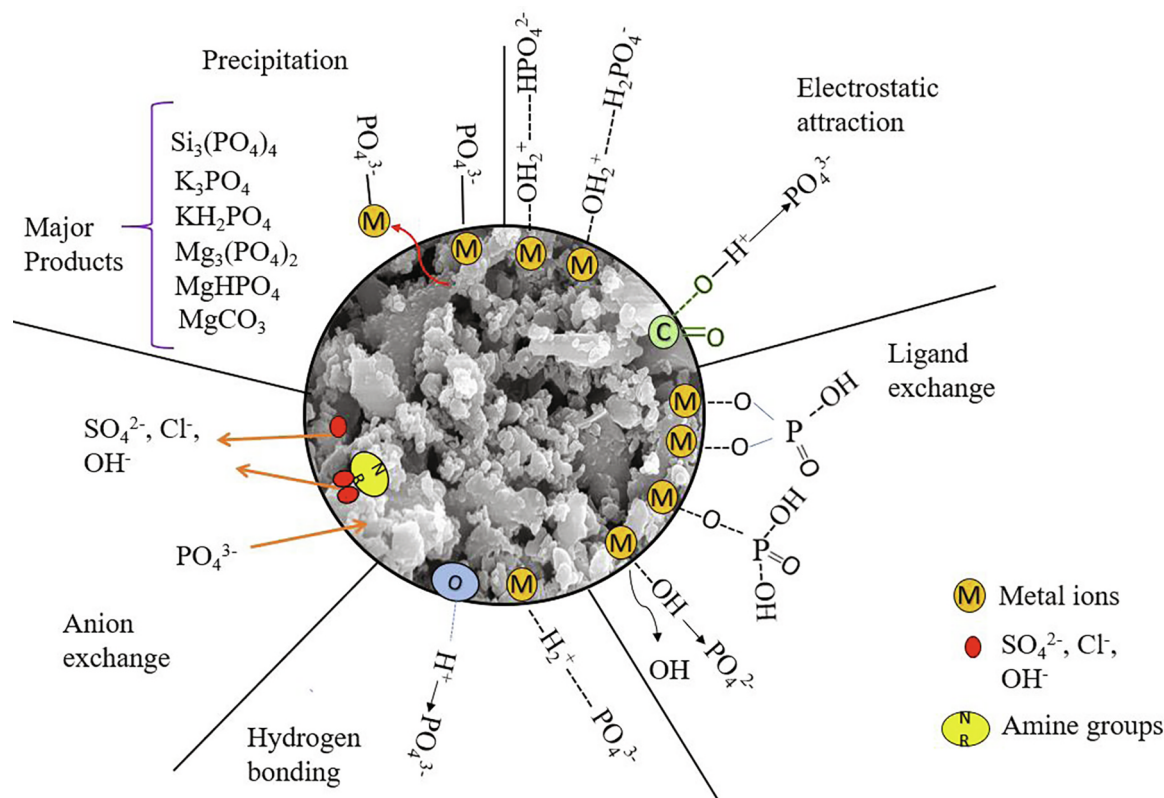


Fig. 13. The Schematic diagrams of various sorption mechanisms of phosphate by BRM in the present study.

and phosphate selectivity also decreased. Ion-exchange, ligand exchange, hydrogen bonding, electrostatic attraction and precipitation, mostly due to the presence of metallic ions in the BRM, were involved in the phosphate adsorption. Phosphate desorption and regeneration was better using NaOH; however, the membrane could be recovered and regenerated with NaCl and showed high phosphate removal efficiency after regeneration. The slow release of phosphate in BRM makes it a good candidate as a slow-release fertilizer. XPS, XRD, FTIR analyses confirmed the successful sorption of phosphate on the adsorbents (BRM and ZnO nanoparticles as comparative adsorbents) and membranes. It was concluded that the results of this study demonstrate that BRM and mixed matrix membranes with BRM offer a promising solution for phosphate adsorption from wastewaters and runoff as part of effective and environmentally sustainable wastewater treatment.

Declaration of Competing Interest

The authors declare that they have no known competing financial interests or personal relationships that could have appeared to influence the work reported in this paper.

Appendix A. Supplementary data

Supplementary data to this article can be found online at <https://doi.org/10.1016/j.cej.2020.126494>.

References

- G.S. Dos Reis, B. Grigore Cazacliu, C. Rodriguez Correa, E. Ovsyannikova, A. Kruse, C. Hoffmann Sampaio, E.C. Lima, G.L. Dotto, Adsorption and recovery of phosphate from aqueous solution by the construction and demolition wastes sludge and its potential use as phosphate-based fertiliser, *J. Environ. Chem. Eng.* (2020), <https://doi.org/10.1016/j.jece.2019.103605>.
- L. Chen, Y. Li, Y. Sun, Y. Chen, J. Qian, La(OH) 3 loaded magnetic mesoporous nanospheres with highly efficient phosphate removal properties and superior pH stability, *Chem. Eng. J.* (2019), <https://doi.org/10.1016/j.cej.2018.11.234>.
- A. Bhatnagar, M. Sillanpää, A review of emerging adsorbents for nitrate removal from water, *Chem. Eng. J.* (2011), <https://doi.org/10.1016/j.cej.2011.01.103>.
- T. Nur, W.G. Shim, P. Loganathan, S. Vigneswaran, J. Kandasamy, Nitrate removal using Purolite A520E ion exchange resin: batch and fixed-bed column adsorption modelling, *Int. J. Environ. Sci. Technol.* (2015), <https://doi.org/10.1007/s13762-014-0510-6>.
- L. Kong, Y. Tian, N. Li, Y. Liu, J. Zhang, J. Zhang, W. Zuo, Highly-effective phosphate removal from aqueous solutions by calcined nano-porous palygorskite matrix with embedded lanthanum hydroxide, *Appl. Clay Sci.* (2018), <https://doi.org/10.1016/j.clay.2018.07.005>.
- C.L. Ritt, B.J. Chisholm, A.N. Bezbaruah, Assessment of molecularly imprinted polymers as phosphate sorbents, *Chemosphere.* (2019), <https://doi.org/10.1016/j.chemosphere.2019.03.087>.
- D. Cordell, J.O. Drangert, S. White, The story of phosphorus: Global food security and food for thought, *Glob. Environ. Chang.* (2009), <https://doi.org/10.1016/j.gloenvcha.2008.10.009>.
- D. Cordell, A. Rosemarin, J.J. Schröder, A.L. Smit, Towards global phosphorus security: A systems framework for phosphorus recovery and reuse options, *Chemosphere.* (2011), <https://doi.org/10.1016/j.chemosphere.2011.02.032>.
- Q. Yuan, J.A. Oleszkiewicz, Biomass fermentation to augment biological phosphorus removal, *Chemosphere.* (2010), <https://doi.org/10.1016/j.chemosphere.2009.09.057>.
- A. Noubli, D.E. Akretche, J.G. Crespo, S. Velizarov, Complementary membrane-based processes for recovery and preconcentration of phosphate from industrial wastewater, *Sep. Purif. Technol.* (2020), <https://doi.org/10.1016/j.seppur.2019.116123>.
- L. Delgadillo-Mirquez, F. Lopes, B. Taidi, D. Pareau, Nitrogen and phosphate removal from wastewater with a mixed microalgae and bacteria culture, *Biotechnol. Reports.* (2016), <https://doi.org/10.1016/j.btre.2016.04.003>.
- H. Monclús, J. Sipma, G. Ferrero, I. Rodríguez-Roda, J. Comas, Biological nutrient removal in an MBR treating municipal wastewater with special focus on biological phosphorus removal, *Bioresour. Technol.* (2010), <https://doi.org/10.1016/j.biortech.2010.01.038>.
- H. Huang, J. Liu, P. Zhang, D. Zhang, F. Gao, Investigation on the simultaneous removal of fluoride, ammonia nitrogen and phosphate from semiconductor wastewater using chemical precipitation, *Chem. Eng. J.* (2017), <https://doi.org/10.1016/j.cej.2016.08.134>.
- H. Huang, D. Zhang, Z. Zhao, P. Zhang, F. Gao, Comparison investigation on phosphate recovery from sludge anaerobic supernatant using the electrocoagulation process and chemical precipitation, *J. Clean. Prod.* (2017), <https://doi.org/10.1016/j.jclepro.2016.09.127>.
- L. Delgadillo-Velasco, V. Hernández-Montoya, M.A. Montes-Morán, R.T. Gómez, F.J. Cervantes, Recovery of different types of hydroxyapatite by precipitation of phosphates of wastewater from anodizing industry, *J. Clean. Prod.* (2020), <https://doi.org/10.1016/j.jclepro.2019.118564>.
- W. Du, Y. Li, X. Xu, Y. Shang, B. Gao, Q. Yue, Selective removal of phosphate by dual Zr and La hydroxide/cellulose-based bio-composites, *J. Colloid Interface Sci.* (2019), <https://doi.org/10.1016/j.jcis.2018.09.002>.
- J. He, W. Wang, F. Sun, W. Shi, D. Qi, K. Wang, R. Shi, F. Cui, C. Wang, X. Chen, Highly Efficient Phosphate Scavenger Based on Well-Dispersed La(OH)₃ Nanorods in Polyacrylonitrile Nanofibers for Nutrient-Starvation Antibacteria, *ACS Nano.* (2015), <https://doi.org/10.1021/acs.nano.5b04236>.
- A. Oehmen, P.C. Lemos, G. Carvalho, Z. Yuan, J. Keller, L.L. Blackall, M.A.M. Reis, Advances in enhanced biological phosphorus removal: From micro to macro scale, *Water Res.* (2007), <https://doi.org/10.1016/j.watres.2007.02.030>.
- D.J. Batstone, T. Hülsen, C.M. Mehta, J. Keller, Platforms for energy and nutrient recovery from domestic wastewater: A review, *Chemosphere.* (2015), <https://doi.org/10.1016/j.chemosphere.2014.10.021>.
- C.M. Mehta, W.O. Khunjar, V. Nguyen, S. Tait, D.J. Batstone, Critical Reviews in Environmental Science and Technology Technologies to Recover Nutrients from Waste Streams: A Critical Review Technologies to Recover Nutrients from Waste Streams: A Critical Review, *Crit. Rev. Environ. Sci. Technol.* (2015), <https://doi.org/10.1080/10643389.2013.866621>.
- S. Zavareh, Z. Behrouzi, A. Avanes, Cu (II) binded chitosan/Fe₃O₄ nanocomposite as a new biosorbent for efficient and selective removal of phosphate, *Int. J. Biol. Macromol.* (2017), <https://doi.org/10.1016/j.ijbiomac.2017.03.074>.
- J.T. Bunce, E. Ndam, I.D. Ofiteru, A. Moore, D.W. Graham, A review of phosphorus removal technologies and their applicability to small-scale domestic wastewater treatment systems, *Front. Environ. Sci.* (2018), <https://doi.org/10.3389/fenvs.2018.00008>.
- S. Rahimi, R.M. Moattari, L. Rajabi, A.A. Derakhshan, Optimization of lead removal from aqueous solution using goethite/chitosan nanocomposite by response surface methodology, *Colloids Surfaces A Physicochem. Eng. Asp.* (2015), <https://doi.org/10.1016/j.colsurfa.2015.07.063>.
- J. Das, B.S. Patra, N. Baliarsingh, K.M. Parida, Adsorption of phosphate by layered double hydroxides in aqueous solutions, *Appl. Clay Sci.* (2006), <https://doi.org/10.1016/j.clay.2006.02.005>.
- Y. Su, W. Yang, W. Sun, Q. Li, J.K. Shang, Synthesis of mesoporous cerium-yttrium binary oxide nanoadsorbents by a solvothermal process and their effective adsorption of phosphate from water, *Chem. Eng. J.* (2015), <https://doi.org/10.1016/j.cej.2015.01.070>.
- L. Chen, X. Zhao, B. Pan, W. Zhang, M. Hua, L. Lv, W. Zhang, Preferable removal of phosphate from water using hydrous zirconium oxide-based nanocomposite of high stability, *J. Hazard. Mater.* (2015), <https://doi.org/10.1016/j.jhazmat.2014.10.048>.
- B. Abebe, A.M. Tadesse, T. Kebede, E. Teju, I. Diaz, Fe-Al-Mn ternary oxide nanosorbent: Synthesis, characterization and phosphate sorption property, *J. Environ. Chem. Eng.* (2017), <https://doi.org/10.1016/j.jece.2017.02.026>.
- Y. Zhang, B. Pan, C. Shan, X. Gao, Enhanced Phosphate Removal by Nanosized Hydrated La(III) Oxide Confined in Cross-linked Polystyrene Networks, *Environ. Sci. Technol.* (2016), <https://doi.org/10.1021/acs.est.5b04630>.
- Z. Liu, W. Wu, Y. Liu, X. Hu, Preparation of surface anion imprinted polymer by developing a La(III)-coordinated 3-methacryloxyethyl-propyl bi-functionalized graphene oxide for phosphate removal, *J. Taiwan Inst. Chem. Eng.* (2018), <https://doi.org/10.1016/j.jtice.2018.02.001>.
- J. Xie, Z. Wang, S. Lu, D. Wu, Z. Zhang, H. Kong, Removal and recovery of phosphate from water by lanthanum hydroxide materials, *Chem. Eng. J.* (2014), <https://doi.org/10.1016/j.cej.2014.05.113>.
- H. Qiu, S. Zhang, B. Pan, W. Zhang, L. Lv, Oxalate-promoted dissolution of hydrous ferric oxide immobilized within nanoporous polymers: Effect of ionic strength and visible light irradiation, *Chem. Eng. J.* (2013), <https://doi.org/10.1016/j.cej.2013.07.092>.
- Y. Shang, X. Xu, S. Qi, Y. Zhao, Z. Ren, B. Gao, Preferable uptake of phosphate by hydrous zirconium oxide nanoparticles embedded in quaternary-ammonium Chinese reed, *J. Colloid Interface Sci.* (2017), <https://doi.org/10.1016/j.jcis.2017.02.019>.
- H. Qiu, Z.F. Qin, F.L. Liu, C. Liang, M.X. Song, Z.W. Xu, Y.D. Guan, Fabrication of a Biomass-Based Hydrous Zirconium Oxide Nanocomposite for Advanced Phosphate Removal, *Huanjing Kexue/Environmental Sci.* (2018), <https://doi.org/10.13227/j.hjkk.201706118>.
- T. Almeelbi, A. Bezbaruah, Aqueous phosphate removal using nanoscale zero-valent iron, in: *Nanotechnol. Sustain. Dev. First Ed.*, 2014. doi:10.1007/978-3-319-05041-6_16.
- J.H. Park, J.J. Wang, R. Xiao, B. Zhou, R.D. Delaune, D.C. Seo, Effect of pyrolysis temperature on phosphate adsorption characteristics and mechanisms of crawfish char, *J. Colloid Interface Sci.* (2018), <https://doi.org/10.1016/j.jcis.2018.04.078>.
- F. Xie, F. Wu, G. Liu, Y. Mu, C. Feng, H. Wang, J.P. Giesy, Removal of phosphate from eutrophic lakes through adsorption by in situ formation of magnesium hydroxide from diatomite, *Environ. Sci. Technol.* (2014), <https://doi.org/10.1021/es4037379>.
- Z. Wang, H. Guo, F. Shen, G. Yang, Y. Zhang, Y. Zeng, L. Wang, H. Xiao, S. Deng, Biochar produced from oak sawdust by Lanthanum (La)-involved pyrolysis for adsorption of ammonium (NH₄⁺), nitrate (NO₃⁻), and phosphate (PO₄⁻), *Chemosphere.* (2015), <https://doi.org/10.1016/j.chemosphere.2014.07.084>.
- J.A. Marshall, B.J. Morton, R. Muhlack, D. Chittleborough, C.W. Kwong, Recovery of phosphate from calcium-containing aqueous solution resulting from biochar-induced calcium phosphate precipitation, *J. Clean. Prod.* (2017), <https://doi.org/>

- 10.1016/j.jclepro.2017.07.042.
- [39] S.V. Novais, M.D.O. Zenero, M.S.C. Barreto, C.R. Montes, C.E.P. Cerri, Phosphorus removal from eutrophic water using modified biochar, *Sci. Total Environ.* (2018), <https://doi.org/10.1016/j.scitotenv.2018.03.246>.
- [40] C.A. Takaya, L.A. Fletcher, S. Singh, U.C. Okwuosa, A.B. Ross, Recovery of phosphate with chemically modified biochars, *J. Environ. Chem. Eng.* (2016), <https://doi.org/10.1016/j.jece.2016.01.011>.
- [41] S.V. Novais, M.D.O. Zenero, J. Tronto, R.F. Conz, C.E.P. Cerri, Poultry manure and sugarcane straw biochars modified with MgCl₂ for phosphorus adsorption, *J. Environ. Manage.* (2018), <https://doi.org/10.1016/j.jenvman.2018.02.088>.
- [42] D. Jiang, B. Chu, Y. Amano, M. Machida, Removal and recovery of phosphate from water by Mg-laden biochar: Batch and column studies, *Colloids Surfaces A Physicochem. Eng. Asp.* (2018), <https://doi.org/10.1016/j.colsurfa.2018.09.016>.
- [43] X. Cui, X. Dai, K.Y. Khan, T. Li, X. Yang, Z. He, Removal of phosphate from aqueous solution using magnesium-alginate/chitosan modified biochar microspheres derived from *Thalia dealbata*, *Bioresour. Technol.* (2016), <https://doi.org/10.1016/j.biortech.2016.07.072>.
- [44] M. Delavar, G. Bakeri, M. Hosseini, Fabrication of polycarbonate mixed matrix membranes containing hydrous manganese oxide and alumina nanoparticles for heavy metal decontamination: Characterization and comparative study, *Chem. Eng. Res. Des.* (2017), <https://doi.org/10.1016/j.cherd.2017.02.029>.
- [45] S. Zare, A. Kargari, Membrane properties in membrane distillation, in: *Emerg. Technol. Sustain. Desalin. Handb.*, 2018. doi:10.1016/B978-0-12-815818-0.00004-7.
- [46] E. Nagy, Basic Equations of the Mass Transport through a Membrane Layer (2012), <https://doi.org/10.1016/C2011-0-04271-0>.
- [47] V. Nayak, M.S. Jyothi, R.G. Balakrishna, M. Padaki, A.F. Ismail, Preparation and Characterization of Chitosan Thin Films on Mixed-Matrix Membranes for Complete Removal of Chromium, *ChemistryOpen*. (2015), <https://doi.org/10.1002/open.201402133>.
- [48] R. Liu, Y. Sui, X. Wang, Metal-organic framework-based ultrafiltration membrane separation with capacitive-type for enhanced phosphate removal, *Chem. Eng. J.* (2019), <https://doi.org/10.1016/j.cej.2019.04.136>.
- [49] R. Mukherjee, P. Bhunia, S. De, Impact of graphene oxide on removal of heavy metals using mixed matrix membrane, *Chem. Eng. J.* (2016), <https://doi.org/10.1016/j.cej.2016.02.015>.
- [50] M.J.C. Ordoñez, K.J. Balkus, J.P. Ferraris, I.H. Musselman, Molecular sieving realized with ZIF-8/Matrimid® mixed-matrix membranes, *J. Memb. Sci.* (2010), <https://doi.org/10.1016/j.memsci.2010.06.017>.
- [51] G. Arthanareeswaran, P. Thanikaivelan, Fabrication of cellulose acetate-zirconia hybrid membranes for ultrafiltration applications: Performance, structure and fouling analysis, *Sep. Purif. Technol.* (2010), <https://doi.org/10.1016/j.seppur.2010.06.010>.
- [52] H. Wang, S. He, X. Qin, C. Li, T. Li, Interfacial Engineering in Metal-Organic Framework-Based Mixed Matrix Membranes Using Covalently Grafted Polyimide Brushes, *J. Am. Chem. Soc.* (2018), <https://doi.org/10.1021/jacs.8b10138>.
- [53] P. Duan, J.C. Moreton, S.R. Tavares, R. Semino, G. Maurin, S.M. Cohen, K. Schmidt-Rohr, Polymer Infiltration into Metal-Organic Frameworks in Mixed-Matrix Membranes Detected in Situ by NMR, *J. Am. Chem. Soc.* (2019), <https://doi.org/10.1021/jacs.9b02789>.
- [54] X. Cheng, X. Huang, X. Wang, B. Zhao, A. Chen, D. Sun, Phosphate adsorption from sewage sludge filtrate using zinc-aluminum layered double hydroxides, *J. Hazard. Mater.* (2009), <https://doi.org/10.1016/j.jhazmat.2009.04.052>.
- [55] J. Zhou, S. Yang, J. Yu, Z. Shu, Novel hollow microspheres of hierarchical zinc-aluminum layered double hydroxides and their enhanced adsorption capacity for phosphate in water, *J. Hazard. Mater.* (2011), <https://doi.org/10.1016/j.jhazmat.2011.06.013>.
- [56] H. He, H. Kang, S. Ma, Y. Bai, X. Yang, High adsorption selectivity of ZnAl layered double hydroxides and the calcined materials toward phosphate, *J. Colloid Interface Sci.* (2010), <https://doi.org/10.1016/j.jcis.2009.11.004>.
- [57] R. Jamshidi Gohari, W.J. Lau, T. Matsuura, E. Halakoo, A.F. Ismail, Adsorptive removal of Pb(II) from aqueous solution by novel PES/HMO ultrafiltration mixed matrix membrane, *Sep. Purif. Technol.* (2013), <https://doi.org/10.1016/j.seppur.2013.09.024>.
- [58] Y. Huang, X. Lee, M. Grattieri, M. Yuan, R. Cai, F.C. Macazo, S.D. Minteer, Modified biochar for phosphate adsorption in environmentally relevant conditions, *Chem. Eng. J.* (2020), <https://doi.org/10.1016/j.cej.2019.122375>.
- [59] M. Nehra, N. Dilbaghi, N.K. Singhal, A.A. Hassan, K.H. Kim, S. Kumar, Metal organic frameworks MIL-100(Fe) as an efficient adsorptive material for phosphate management, *Environ. Res.* (2019), <https://doi.org/10.1016/j.envres.2018.11.013>.
- [60] A. Behboudi, Y. Jafarzadeh, R. Yegani, Preparation and characterization of TiO₂ embedded PVC ultrafiltration membranes, *Chem. Eng. Res. Des.* (2016), <https://doi.org/10.1016/j.cherd.2016.07.027>.
- [61] S.M. Hosseini, S.H. Amini, A.R. Khodabakhshi, E. Bagheripour, B. Van der Bruggen, Activated carbon nanoparticles entrapped mixed matrix polyethersulfone based nanofiltration membrane for sulfate and copper removal from water, *J. Taiwan Inst. Chem. Eng.* (2018), <https://doi.org/10.1016/j.jtice.2017.11.017>.
- [62] S. Zhao, W. Yan, M. Shi, Z. Wang, J. Wang, S. Wang, Improving permeability and antifouling performance of polyethersulfone ultrafiltration membrane by incorporation of ZnO-DMF dispersion containing nano-ZnO and polyvinylpyrrolidone, *J. Memb. Sci.* (2015), <https://doi.org/10.1016/j.memsci.2014.12.050>.
- [63] S. Chandra, I. Medha, J. Bhattacharya, Potassium-iron rice straw biochar composite for sorption of nitrate, phosphate, and ammonium ions in soil for timely and controlled release, *Sci. Total Environ.* (2020), <https://doi.org/10.1016/j.scitotenv.2019.136337>.
- [64] L. Zhao, X. Cao, Q. Wang, F. Yang, S. Xu, Mineral Constituents Profile of Biochar Derived from Diversified Waste Biomasses: Implications for Agricultural Applications, *J. Environ. Qual.* (2013), <https://doi.org/10.2134/jeq2012.0232>.
- [65] L. Dai, F. Tan, H. Li, N. Zhu, M. He, Q. Zhu, G. Hu, L. Wang, J. Zhao, Calcium-rich biochar from the pyrolysis of crab shell for phosphorus removal, *J. Environ. Manage.* (2017), <https://doi.org/10.1016/j.jenvman.2017.04.057>.
- [66] C.A. Takaya, L.A. Fletcher, S. Singh, K.U. Anyikude, A.B. Ross, Phosphate and ammonium sorption capacity of biochar and hydrochar from different wastes, *Chemosphere.* (2016), <https://doi.org/10.1016/j.chemosphere.2015.11.052>.
- [67] S.M. Shaheen, N.K. Niazi, N.E.E. Hassan, I. Bibi, H. Wang, D.C.W. Tsang, Y.S. Ok, N. Bolan, J. Rinklebe, Wood-based biochar for the removal of potentially toxic elements in water and wastewater: a critical review, *Int. Mater. Rev.* (2019), <https://doi.org/10.1080/09506608.2018.1473096>.
- [68] M. Vithanage, I. Herath, S. Joseph, J. Bundschuh, N. Bolan, Y.S. Ok, M.B. Kirkham, J. Rinklebe, Interaction of arsenic with biochar in soil and water: A critical review, *Carbon N. Y.* (2017), <https://doi.org/10.1016/j.carbon.2016.11.032>.
- [69] M. Ahmad, S.S. Lee, X. Dou, D. Mohan, J.K. Sung, J.E. Yang, Y.S. Ok, Effects of pyrolysis temperature on soybean stover- and peanut shell-derived biochar properties and TCE adsorption in water, *Bioresour. Technol.* (2012), <https://doi.org/10.1016/j.biortech.2012.05.042>.
- [70] A.W. Samsuri, F. Sadegh-Zadeh, B.J. Seh-Bardan, Characterization of biochars produced from oil palm and rice husks and their adsorption capacities for heavy metals, *Int. J. Environ. Sci. Technol.* (2014), <https://doi.org/10.1007/s13762-013-0291-3>.
- [71] M.K. Rafiq, R.T. Bachmann, M.T. Rafiq, Z. Shang, S. Joseph, R.L. Long, Influence of pyrolysis temperature on physico-chemical properties of corn stover (zea mays L.) biochar and feasibility for carbon capture and energy balance, *PLoS One.* (2016), <https://doi.org/10.1371/journal.pone.0156894>.
- [72] D.L. Ramasamy, V. Puhakka, B. Doshi, S. Iftikhar, M. Sillanpää, Fabrication of carbon nanotubes reinforced silica composites with improved rare earth elements adsorption performance, *Chem. Eng. J.* (2019), <https://doi.org/10.1016/j.cej.2019.02.057>.
- [73] W. Zheng, Using Biochar as a Soil Amendment for Sustainable Agriculture, *Sustain, Agric.*, 2010.
- [74] M.T. Amin, A.A. Alazba, M. Shafiq, Effective adsorption of methylene blue dye using activated carbon developed from the rosemary plant: Isotherms and kinetic studies, *Desalin. Water Treat.* (2017), <https://doi.org/10.5004/dwt.2017.20572>.
- [75] M. Erhayem, F. Al-Tohami, R. Mohamed, K. Ahmida, Isotherm, Kinetic and Thermodynamic Studies for the Sorption of Mercury (II) onto Activated Carbon from < i > Rosmarinus officinalis < / i > Leaves, *Am. J. Anal. Chem.* (2015), <https://doi.org/10.4236/ajac.2015.61001>.
- [76] L. Berzina-Cimdina, N. Borodajenko, Research of Calcium Phosphates Using Fourier Transform Infrared Spectroscopy, in: *Infrared Spectrosc. - Mater. Sci. Eng. Technol.*, 2012. doi:10.5772/36942.
- [77] Q. Gao, C.Z. Wang, S. Liu, D. Hanigan, S.T. Liu, H.Z. Zhao, Ultrafiltration membrane microreactor (MMR) for simultaneous removal of nitrate and phosphate from water, *Chem. Eng. J.* (2019), <https://doi.org/10.1016/j.cej.2018.08.137>.
- [78] A. Roguska, M. Pisarek, M. Andrzejczuk, M. Dolata, M. Lewandowska, M. Janik-Czachor, Characterization of a calcium phosphate-TiO₂ nanotube composite layer for biomedical applications, *Mater. Sci. Eng. C.* (2011), <https://doi.org/10.1016/j.msec.2011.02.009>.
- [79] K. Allam, A. El Bouari, B. Belhorma, L. Bih, Removal of Methylene Blue from Water Using Hydroxyapatite Submitted to Microwave Irradiation, *J. Water Resour. Prot.* (2016), <https://doi.org/10.4236/jwarp.2016.83030>.
- [80] J.H. Kim, S.H. Kim, H.K. Kim, T. Akaikie, S.C. Kim, Synthesis and characterization of hydroxyapatite crystals: A review study on the analytical methods, *J. Biomed. Mater. Res.* (2002), <https://doi.org/10.1002/jbm.10280>.
- [81] L. He, G. Dong, C. Deng, Effects of strontium substitution on the phase transformation and crystal structure of calcium phosphate derived by chemical precipitation, *Ceram. Int.* (2016), <https://doi.org/10.1016/j.ceramint.2016.04.116>.
- [82] D. Pathania, S. Sharma, P. Singh, Removal of methylene blue by adsorption onto activated carbon developed from *Ficus carica* bast, *Arab. J. Chem.* (2017), <https://doi.org/10.1016/j.arabjc.2013.04.021>.
- [83] L.A. Malik, A. Bashir, T. Manzoor, A.H. Pandith, Microwave-assisted synthesis of glutathione-coated hollow zinc oxide for the removal of heavy metal ions from aqueous systems, *RSC Adv.* (2019), <https://doi.org/10.1039/c9ra00243j>.
- [84] A.C. Arulrajana, D.L. Ramasamy, M. Sillanpää, A. van der Wal, P.M. Biesheuvel, S. Porada, J.E. Dykstra, Exceptional Water Desalination Performance with Anion-Selective Electrodes, *Adv. Mater.* (2019), <https://doi.org/10.1002/adma.201806937>.
- [85] Y. Liu, X. Zhao, J. Li, D. Ma, R. Han, Characterization of bio-char from pyrolysis of wheat straw and its evaluation on methylene blue adsorption, *Desalin. Water Treat.* (2012), <https://doi.org/10.1080/19443994.2012.677408>.
- [86] P.V. and I.V.P. M. Kandiban, Synthesis and Characterization of Mgo Nanoparticles for Photocatalytic, Conference. (2015) 1–5.
- [87] J. Zhang, B. Huang, L. Chen, J. Du, W. Li, Z. Luo, Pyrolysis kinetics of hulls barley straw using the distributed activation energy model (DAEM) by the TG/DTA technique and SEM/XRD characterizations for hulls barley straw derived biochar, *Brazilian J. Chem. Eng.* (2018), <https://doi.org/10.1590/0104-6632.20180353s20170382>.
- [88] A. Elavarasan, EDX AND XRD, FT-IR SPECTRA, ANALYSIS CONTAINING HEXAVALENT CHROMIUM METAL ION ADSORPTION PRESENT IN AQUEOUS SOLUTION ON TO PHOSPHORIC ACID (H3PO4) ACTIVATED MIMUSOPUS ELENGI LEAVES CARBON, *J. Drug Deliv. Ther.* (2018), <https://doi.org/10.22270/jddt>.

- v8i5-s.1917.
- [89] P. Patra, S. Mitra, N. Debnath, P. Pramanik, A. Goswami, Ciprofloxacin conjugated zinc oxide nanoparticle: A camouflage towards multidrug resistant bacteria, *Bull. Mater. Sci.* (2014), <https://doi.org/10.1007/s12034-014-0637-6>.
- [90] D. Raoufi, Synthesis and microstructural properties of ZnO nanoparticles prepared by precipitation method, *Renew. Energy*. (2013), <https://doi.org/10.1016/j.renene.2012.08.076>.
- [91] B.N. Patil, T.C. Taranath, Limonia acidissima L. leaf mediated synthesis of zinc oxide nanoparticles: A potent tool against Mycobacterium tuberculosis, *Int. J. Mycobacteriology*. (2016), <https://doi.org/10.1016/j.ijmyco.2016.03.004>.
- [92] Z. Luo, S. Zhu, Z. Liu, J. Liu, M. Huo, W. Yang, Study of phosphate removal from aqueous solution by zinc oxide, *J. Water Health*. (2015), <https://doi.org/10.2166/wh.2015.210>.
- [93] K.L. Bae, J. Kim, C.K. Lim, K.M. Nam, H. Song, Colloidal zinc oxide-copper(I) oxide nanocatalysts for selective aqueous photocatalytic carbon dioxide conversion into methane, *Nat. Commun.* (2017), <https://doi.org/10.1038/s41467-017-01165-4>.
- [94] S. Xu, T. Sun, Q. Xu, C. Duan, Y. Dai, L. Wang, Q. Song, Preparation and Antibiofilm Properties of Zinc Oxide/Porous Anodic Alumina Composite Films, *Nanoscale Res. Lett.* (2018), <https://doi.org/10.1186/s11671-018-2568-4>.
- [95] A.N. Kadam, D.P. Bhopate, V.V. Kondalkar, S.M. Majhi, C.D. Bathula, A.V. Tran, S.W. Lee, Facile synthesis of Ag-ZnO core-shell nanostructures with enhanced photocatalytic activity, *J. Ind. Eng. Chem.* (2018), <https://doi.org/10.1016/j.jiec.2017.12.003>.
- [96] L. Leng, S. Xu, R. Liu, T. Yu, X. Zhuo, S. Leng, Q. Xiong, H. Huang, Nitrogen containing functional groups of biochar: An overview, *Bioresour. Technol.* (2019), <https://doi.org/10.1016/j.biortech.2019.122286>.
- [97] B. Vincent Crist, Handbooks of Monochromatic XPS Spectra Volume 1 - The Elements and Native Oxides, *Handb. Elem. Nativ. Oxides*. (1999), <https://doi.org/10.1002/pspb.2221980103>.
- [98] R. Al-Gaashani, S. Radiman, A.R. Daud, N. Tabet, Y. Al-Douri, XPS and optical studies of different morphologies of ZnO nanostructures prepared by microwave methods, *Ceram. Int.* (2013), <https://doi.org/10.1016/j.ceramint.2012.08.075>.
- [99] J.H. Zheng, Q. Jiang, J.S. Lian, Synthesis and optical properties of flower-like ZnO nanorods by thermal evaporation method, *Appl. Surf. Sci.* (2011), <https://doi.org/10.1016/j.apsusc.2011.01.025>.
- [100] H. Zhou, Z. Li, Synthesis of nanowires, nanorods and nanoparticles of ZnO through modulating the ratio of water to methanol by using a mild and simple solution method, *Mater. Chem. Phys.* (2005), <https://doi.org/10.1016/j.matchemphys.2004.09.006>.
- [101] A. Abdelhay, A. Al Bsoul, A. Al-Othman, N.M. Al-Ananzeh, I. Jum'ah, A.A. Al-Taani, Kinetic and thermodynamic study of phosphate removal from water by adsorption onto (Arundo donax) reeds, *Adsorpt. Sci. Technol.* (2018). doi:10.1177/0263617416684347.
- [102] L. de Castro, V. Brandão, L. Bertolino, W. de Souza, V. Teixeira, Phosphate Adsorption by Montmorillonites Modified with Lanthanum/Iron and a Laboratory Test using Water from the Jacarepaguá Lagoon (RJ, Brazil), *J. Braz. Chem. Soc.* (2018), <https://doi.org/10.21577/0103-5053.20180236>.
- [103] Z. Zha, Y. Ren, S. Wang, Z. Qian, L. Yang, P. Cheng, Y. Han, M. Wang, Phosphate adsorption onto thermally dehydrated aluminate cement granules, *RSC Adv.* (2018), <https://doi.org/10.1039/c8ra02474j>.
- [104] I. Anastopoulos, A. Bhatnagar, E.C. Lima, Adsorption of rare earth metals: A review of recent literature, *J. Mol. Liq.* (2016), <https://doi.org/10.1016/j.molliq.2016.06.076>.
- [105] V.K. Gupta, S. Agarwal, H. Sadegh, G.A.M. Ali, A.K. Bharti, A.S. Hamdy Makhlof, Facile route synthesis of novel graphene oxide- β -cyclodextrin nanocomposite and its application as adsorbent for removal of toxic bisphenol A from the aqueous phase, *J. Mol. Liq.* (2017), <https://doi.org/10.1016/j.molliq.2017.04.113>.
- [106] K.W. Jung, M.J. Hwang, K.H. Ahn, Y.S. Ok, Kinetic study on phosphate removal from aqueous solution by biochar derived from peanut shell as renewable adsorptive media, *Int. J. Environ. Sci. Technol.* (2015), <https://doi.org/10.1007/s13762-015-0766-5>.
- [107] Y.W. Berkessa, S.T. Mereta, F.F. Feyisa, Simultaneous removal of nitrate and phosphate from wastewater using solid waste from factory, *Appl. Water Sci.* (2019), <https://doi.org/10.1007/s13201-019-0906-z>.
- [108] T. Liao, T. Li, X. Su, X. Yu, H. Song, Y. Zhu, Y. Zhang, La(OH)₃-modified magnetic pineapple biochar as novel adsorbents for efficient phosphate removal, *Bioresour. Technol.* (2018), <https://doi.org/10.1016/j.biortech.2018.04.108>.
- [109] S. Chatterjee, S. De, Adsorptive removal of fluoride by activated alumina doped cellulose acetate phthalate (CAP) mixed matrix membrane, *Sep. Purif. Technol.* (2014), <https://doi.org/10.1016/j.seppur.2014.01.055>.
- [110] L. Fang, J. shan Li, S. Donatello, C.R. Cheeseman, C.S. Poon, D.C.W. Tsang, Use of Mg/Ca modified biochars to take up phosphorus from acid-extract of incinerated sewage sludge ash (ISSA) for fertilizer application, *J. Clean. Prod.* (2020). doi:10.1016/j.jclepro.2019.118853.
- [111] Z. Wang, D. Shen, F. Shen, T. Li, Phosphate adsorption on lanthanum loaded biochar, *Chemosphere*. (2016), <https://doi.org/10.1016/j.chemosphere.2016.02.004>.
- [112] B. Chen, Z. Chen, S. Lv, A novel magnetic biochar efficiently sorbs organic pollutants and phosphate, *Bioresour. Technol.* (2011), <https://doi.org/10.1016/j.biortech.2010.08.067>.
- [113] Z. Wang, E. Nie, J. Li, M. Yang, Y. Zhao, X. Luo, Z. Zheng, Equilibrium and kinetics of adsorption of phosphate onto iron-doped activated carbon, *Environ. Sci. Pollut. Res.* (2012), <https://doi.org/10.1007/s11356-012-0799-y>.
- [114] J.H. Park, Y.S. Ok, S.H. Kim, J.S. Cho, J.S. Heo, R.D. Delaune, D.C. Seo, Evaluation of phosphorus adsorption capacity of sesame straw biochar on aqueous solution: influence of activation methods and pyrolysis temperatures, *Environ. Geochem.* (2015), <https://doi.org/10.1007/s10653-015-9709-9>.
- [115] J. Ren, N. Li, L. Li, J.K. An, L. Zhao, N.Q. Ren, Granulation and ferric oxides loading enable biochar derived from cotton stalk to remove phosphate from water, *Bioresour. Technol.* (2015), <https://doi.org/10.1016/j.biortech.2014.09.071>.
- [116] A. Aldawsari, M.A. Khan, B.H. Hameed, A.A. Alqadami, M.R. Siddiqui, Z.A. Allothman, A.Y.B.H. Ahmed, Mercerized mesoporous date pit activated carbon - A novel adsorbent to sequester potentially toxic divalent heavy metals from water, *PLoS One*. (2017), <https://doi.org/10.1371/journal.pone.0184493>.
- [117] H. Babelo, A.M.A. Pintor, S.C.R. Santos, R.A.R. Boaventura, C.M.S. Botelho, Performance and prospects of different adsorbents for phosphorus uptake and recovery from water, *Chem. Eng. J.* (2020), <https://doi.org/10.1016/j.cej.2019.122566>.
- [118] L. guo Yan, K. Yang, R. ran Shan, T. Yan, J. Wei, S. jun Yu, H. qin Yu, B. Du, Kinetic, isotherm and thermodynamic investigations of phosphate adsorption onto core-shell Fe₃O₄/LDHs composites with easy magnetic separation assistance, *J. Colloid Interface Sci.* (2015). doi:10.1016/j.jcis.2015.02.048.
- [119] N. Wang, J. Feng, J. Chen, J. Wang, W. Yan, Adsorption mechanism of phosphate by polyaniline/TiO₂ composite from wastewater, *Chem. Eng. J.* (2017), <https://doi.org/10.1016/j.cej.2017.01.066>.
- [120] J. Choi, J. Chung, W. Lee, J.O. Kim, Phosphorous adsorption on synthesized magnetite in wastewater, *J. Ind. Eng. Chem.* (2016), <https://doi.org/10.1016/j.jiec.2015.11.008>.
- [121] G. Li, S. Gao, G. Zhang, X. Zhang, Enhanced adsorption of phosphate from aqueous solution by nanostructured iron(III)-copper(II) binary oxides, *Chem. Eng. J.* (2014), <https://doi.org/10.1016/j.cej.2013.09.021>.
- [122] K.R. Hall, L.C. Eagleton, A. Acrivos, T. Vermeulen, Pore- and solid-diffusion kinetics in fixed-bed adsorption under constant-pattern conditions, *Ind. Eng. Chem. Fundam.* (1966), <https://doi.org/10.1021/i160018a011>.
- [123] A. Özer, H.B. Pirinççi, The adsorption of Cd(II) ions on sulphuric acid-treated wheat bran, *J. Hazard. Mater.* (2006), <https://doi.org/10.1016/j.jhazmat.2006.03.009>.
- [124] J. Li, B. Li, H. Huang, X. Lv, N. Zhao, G. Guo, D. Zhang, Removal of phosphate from aqueous solution by dolomite-modified biochar derived from urban dewatered sewage sludge, *Sci. Total Environ.* (2019), <https://doi.org/10.1016/j.scitotenv.2019.05.400>.
- [125] Q. Xu, Z. Chen, Z. Wu, F. Xu, D. Yang, Q. He, G. Li, Y. Chen, Novel lanthanum doped biochars derived from lignocellulosic wastes for efficient phosphate removal and regeneration, *Bioresour. Technol.* (2019), <https://doi.org/10.1016/j.biortech.2019.121600>.
- [126] J. Lü, H. Liu, R. Liu, X. Zhao, L. Sun, J. Qu, Adsorptive removal of phosphate by a nanostructured Fe-Al-Mn trimetal oxide adsorbent, *Powder Technol.* (2013), <https://doi.org/10.1016/j.powtec.2012.08.024>.
- [127] R. Li, J.J. Wang, B. Zhou, M.K. Awasthi, A. Ali, Z. Zhang, L.A. Gaston, A.H. Lahori, A. Mahar, Enhancing phosphate adsorption by Mg/Al layered double hydroxide functionalized biochar with different Mg/Al ratios, *Sci. Total Environ.* (2016), <https://doi.org/10.1016/j.scitotenv.2016.03.151>.
- [128] H.T. Banu, S. Meenakshi, One pot synthesis of chitosan grafted quaternized resin for the removal of nitrate and phosphate from aqueous solution, *Int. J. Biol. Macromol.* (2017), <https://doi.org/10.1016/j.ijbiomac.2017.03.043>.
- [129] Q. Yin, B. Zhang, R. Wang, Z. Zhao, Biochar as an adsorbent for inorganic nitrogen and phosphorus removal from water: a review, *Environ. Sci. Pollut. Res.* (2017), <https://doi.org/10.1007/s11356-017-0338-y>.
- [130] M. Li, J. Liu, Y. Xu, G. Qian, Phosphate adsorption on metal oxides and metal hydroxides: A comparative review, *Environ. Rev.* (2016), <https://doi.org/10.1139/er-2015-0080>.
- [131] Z. Tan, S. Yuan, M. Hong, L. Zhang, Q. Huang, Mechanism of negative surface charge formation on biochar and its effect on the fixation of soil Cd, *J. Hazard. Mater.* (2020), <https://doi.org/10.1016/j.jhazmat.2019.121370>.
- [132] J.H. Yuan, R.K. Xu, The amelioration effects of low temperature biochar generated from nine crop residues on an acidic Ultisol, *Soil Use Manag.* (2011), <https://doi.org/10.1111/j.1475-2743.2010.00317.x>.
- [133] F. Qi, Y. Yan, D. Lamb, R. Naidu, N.S. Bolan, Y. Liu, Y.S. Ok, S.W. Donne, K.T. Semple, Thermal stability of biochar and its effects on cadmium sorption capacity, *Bioresour. Technol.* (2017), <https://doi.org/10.1016/j.biortech.2017.07.033>.
- [134] L. Qian, M. Chen, B. Chen, Competitive adsorption of cadmium and aluminum onto fresh and oxidized biochars during aging processes, *J. Soils Sediments*. (2015), <https://doi.org/10.1007/s11368-015-1073-y>.
- [135] G. Bakeri, A.F. Ismail, M. Shariaty-Niassar, T. Matsuura, Effect of polymer concentration on the structure and performance of polyetherimide hollow fiber membranes, *J. Memb. Sci.* (2010), <https://doi.org/10.1016/j.memsci.2010.07.018>.
- [136] R. Jamshidi Gohari, W.J. Lau, T. Matsuura, A.F. Ismail, Fabrication and characterization of novel PES/Fe-Mn binary oxide UF mixed matrix membrane for adsorptive removal of As(III) from contaminated water solution, *Sep. Purif. Technol.* (2013), <https://doi.org/10.1016/j.seppur.2013.06.043>.
- [137] C. Zhang, Y. Mu, W. Zhang, S. Zhao, Y. Wang, PVC-based hybrid membranes containing metal-organic frameworks for Li⁺/Mg²⁺ separation, *J. Memb. Sci.* (2020), <https://doi.org/10.1016/j.memsci.2019.117724>.
- [138] J. He, J.P. Chen, Cu(II)-imprinted poly(vinyl alcohol)/poly(acrylic acid) membrane for greater enhancement in sequestration of copper ion in the presence of competitive heavy metal ions: Material development, process demonstration, and study of mechanisms, *Ind. Eng. Chem. Res.* (2014), <https://doi.org/10.1021/ie5032875>.
- [139] R. Mukherjee, S. De, Preparation of polysulfone titanium di oxide mixed matrix hollow fiber membrane and elimination of long term fouling by in situ

- photoexcitation during filtration of phenolic compounds, *Chem. Eng. J.* (2016), <https://doi.org/10.1016/j.cej.2016.05.060>.
- [140] Z. Jia, S. Hao, X. Lu, Exfoliated Mg–Al–Fe layered double hydroxides/polyether sulfone mixed matrix membranes for adsorption of phosphate and fluoride from aqueous solutions, *J. Environ. Sci. (China)*. (2018), <https://doi.org/10.1016/j.jes.2017.11.012>.
- [141] S. Chatterjee, S. De, Adsorptive removal of arsenic from groundwater using chemically treated iron ore slime incorporated mixed matrix hollow fiber membrane, *Sep. Purif. Technol.* (2017), <https://doi.org/10.1016/j.seppur.2017.02.019>.
- [142] W. Jiang, L. Lin, X. Xu, H. Wang, P. Xu, Physicochemical and electrochemical characterization of cation-exchange membranes modified with polyethyleneimine for elucidating enhanced monovalent permselectivity of electrodialysis, *J. Memb. Sci.* (2019), <https://doi.org/10.1016/j.memsci.2018.11.038>.
- [143] R. Li, J.J. Wang, B. Zhou, M.K. Awasthi, A. Ali, Z. Zhang, A.H. Lahori, A. Mahar, Recovery of phosphate from aqueous solution by magnesium oxide decorated magnetic biochar and its potential as phosphate-based fertilizer substitute, *Bioresour. Technol.* (2016), <https://doi.org/10.1016/j.biortech.2016.02.125>.
- [144] S. Kizito, H. Luo, S. Wu, Z. Ajmal, T. Lv, R. Dong, Phosphate recovery from liquid fraction of anaerobic digestate using four slow pyrolyzed biochars: Dynamics of adsorption, desorption and regeneration, *J. Environ. Manage.* (2017), <https://doi.org/10.1016/j.jenvman.2017.06.057>.
- [145] Y. Zhang, Z. Li, I.B. Mahmood, Recovery of NH₄⁺ by corn cob produced biochars and its potential application as soil conditioner, *Front. Environ. Sci. Eng.* (2014), <https://doi.org/10.1007/s11783-014-0682-9>.
- [146] Q. Yin, M. Liu, H. Ren, Biochar produced from the co-pyrolysis of sewage sludge and walnut shell for ammonium and phosphate adsorption from water, *J. Environ. Manage.* (2019), <https://doi.org/10.1016/j.jenvman.2019.109410>.
- [147] Z. Zeng, S. Da Zhang, T.Q. Li, F.L. Zhao, Z.L. He, H.P. Zhao, X.E. Yang, H.L. Wang, J. Zhao, M.T. Rafiq, Sorption of ammonium and phosphate from aqueous solution by biochar derived from phytoremediation plants, *J. Zhejiang Univ. Sci. B.* (2013), <https://doi.org/10.1631/jzus.B1300102>.
- [148] Y. Yao, B. Gao, J. Chen, L. Yang, Engineered biochar reclaiming phosphate from aqueous solutions: Mechanisms and potential application as a slow-release fertilizer, *Environ. Sci. Technol.* (2013), <https://doi.org/10.1021/es4012977>.
- [149] Y. Yao, B. Gao, M. Inyang, A.R. Zimmerman, X. Cao, P. Pullammanappallil, L. Yang, Removal of phosphate from aqueous solution by biochar derived from anaerobically digested sugar beet tailings, *J. Hazard. Mater.* (2011), <https://doi.org/10.1016/j.jhazmat.2011.03.083>.